TECHNISCHE UNIVERSITÄT WIEN
Vienna University of Technology

ILSB

Diploma Thesis

Comparing the mechanical performance of a new VetWelding® anchor system to a standard suture system for trauma therapy of the ruptured feline Achilles tendon

carried out for the purpose of obtaining the degree of Dipl.-Ing. submitted at TU Wien, Faculty of Mechanical and Industrial Engineering, by

Felix Groß

Mat.Nr.: 01425347

under the supervision of

Univ.Prof. Dipl.Ing. Dr.sc.nat Philipp J. Thurner
Dipl.-Ing. Katja Haslinger
Institute of Lightweight Design and Structural Biomechanics, E317

Vienna, January, 2023

Affidavit

I declare in lieu of oath, that I wrote this thesis and performed the associated research myself, using only literature cited in this volume. If text passages from sources are used literally, they are marked as such.

I confirm that this work is original and has not been submitted elsewhere for any examination, nor is it currently under consideration for a thesis elsewhere.

I acknowledge that the submitted work will be checked electronically-technically using suitable and state-of-the-art means (plagiarism detection software). On the one hand, this ensures that the submitted work was prepared according to the high-quality standards within the applicable rules to ensure good scientific practice "Code of Conduct" at the TU Wien. On the other hand, a comparison with other students' theses avoids violations of my personal copyright.

Vienna, January, 2023

Felix Groß

Acknowledgements

I would like to thank all members of the ILSB who supported me during the project for my thesis.

Especially, I would like to express my gratitude to my supervisors Professor Philipp Thurner and Katja Haslinger for their patient, motivating, and always very helpful support during the last year.

I also want to thank Manuela Meyers, representing VetWelding, and Dr. Riccarda Schünemann for the ongoing feedback throughout the project and for the sample preparation.

Special thanks go to my family, who always supported me during my studies and in life. This would not have been possible without them and all of my friends.

Abstract

In this work, a standard intra-osseous suture method was biomechanically compared to a new anchor method of tendon re-fixation by in-vitro tensile testing of feline Achilles tendon samples.

A functional interface between bone and tendon is crucial to ensure load transmission and therefore the skeletal motion in all mammals. For cats, the standard procedure for therapy of an Achilles tendon avulsion is suturing the tendon to an intra-osseous tunnel, pre-drilled in the distal calcaneus. An alternative to the tunnel suture is the application of a suture anchor, implanted into the calcaneus. Exemplary, the thermoplastic VetWelding Weldix® anchor can be stimulated by applying ultrasonic energy, making the material mold exactly into the bone structure and leading to a high primary stability compared to other anchor systems.

The objective of this study is the investigation of gap development between bone and tendon upon tension, as extensive gap formation can hinder the healing of the repaired site.

Results show that samples that were prepared by suture anchor develop a significantly smaller gap compared to samples that were prepared by the intra-osseous tunnel when exposed to the same load. A reference gap of 0.5 mm is reached within the intra-osseous group at a mean tendon load of (23.0 ± 15.4) N, while anchor samples needed almost double the load with a mean of (44.2 ± 5.5) N to reach the same gap-size. This means that the use of a suture anchor leads to less disturbance of the repaired bone-tendon interface and might improve the healing process. At the same time, the maximum load before suture failure is comparable between both groups.

This work shows that the biomechanical properties of the VetWelding Weldix® suture anchor are favorable compared to the state-of-the-art intra-osseous tunnel method. For better statistical analysis, more tests can be done in the future, especially a pairwise analysis would require more samples.

Contents

List of Figures

List of Tables

Chapter 1

Introduction

1.1 Background and Motivation

A functional bone-tendon interface is crucial to ensure the physiological transmission of forces between muscle and bone for locomotion in all mammals. Tendon damage can lead to pain, muscle or tendon injuries, and ultimately to a reduced range of motion. Tendon injuries in pets are generally quite rare and are mostly caused by trauma, however, they do occur regularly [1]. Therapy of these injuries in veterinary medicine can be complicated and expensive, so the development of new and easy-to-handle therapy methods is important.

Depending on the severity of tendon damage, different therapy methods are applied. Conservative therapy can ease pain in some cases [2], but cannot restore the full load-bearing capacity of more severely affected tendons. In case of a complete rupture, therapy depends on the exact injury location. Ruptures in the middle region of a tendon can be sutured back together using both ends of the injured tendon. Cases of ruptured tendons close to the bone-tendon interface can be directly fixed back onto the bone, using different orthopedic procedures [1].

Veterinary orthopedics currently mostly relies on intra-osseous sutures for such cases. Here, a tunnel is drilled through the bone at the site of the rupture. A suture is passed through the tunnel and the ruptured tendon is sutured back onto the bone [3, 4].

In human medicine, the use of suture anchor systems has been state-of-the-art for years for tendon ruptures close to their insertion [5]. These small, cylindrical bone implants are fixed at the site of the original tendon insertion, already carrying the sutures to re-fixate ruptured tendons. Suture anchor systems have proven themselves in terms of usability over the years. Studies also show their good mechanical performance, suggesting that the healing process of ruptured tendons repaired by suture anchors might be better compared to the healing of intra-osseous sutures [6].

In an attempt to use the advantages of suture anchors also in veterinary orthopedics, VetWelding developed a suture anchor. It is smaller than most anchor systems used in veterinary medicine and can be applied even in delicate bones. Its BoneWelding® technology enables the anchor to be molded into a small pre-drilled hole at the insertion site. Upon ultrasonic excitation, the thermoplastic material melts and penetrates the trabecular structure beneath the layer of cortical bone, leading to a high primary stability of the implant [7]. An application of this system is the repair of the feline Achilles tendon.

In a study on ruptured canine Achilles tendon samples, Moores et al. [8] compared different suturing techniques, combined with the intra-osseous suture. It was found, that the gap between bone and tendon can grow to more than 3 mm upon load. According to Gelberman et al. [9], gaps of that magnitude can already negatively influence the tendon's healing process. In order to minimize gap formation, alternative methods for tendon re-fixation to bone need to be explored.

1.2 Goals of the Thesis

The goal of this work is to create a better understanding of different tendon reattachment methods, in particular, to compare the mechanical properties of the trans-osseous suture with the mechanical properties of the VetWelding Weldix® suture anchor for Achilles tendon repair in feline samples. Specifically, the aims of this thesis are:

(i) Establishment of a testing protocol using an experimental setup, including micro-computed tomography (µCT) imaging and tensile testing machine.

(ii) Execution of tests on 10 pairs of feline Achilles tendon samples, respectively one sample prepared by tunnel suture and one sample prepared by bone anchor.

(iii) Analysis of the results and comparison of both therapy methods.

1.3 Structure of the Thesis

Chapter 2 describes the structural and biomechanical properties of the bone-tendon interface. After introducing the biological materials of bone and tendon themselves and going into more detail on the hierarchical structure of both, the tendon insertion into bone is explained by highlighting the four zones of the enthesis.

In the first part of Chapter 3, the anatomy of the feline hind leg is presented. Then, orthopedic methods of tendon reconstruction are explained, taking into account a variety of suturing techniques. The intra-osseous suture method is shown and su-

ture anchor systems are introduced by describing different implantation principles and material choices.

In Chapter 4, the materials and methods used for the experiments are described. This includes the procedures of both methods for sample preparation, the intra-osseous suture and the suture anchor. The custom-made experimental setup is explained as well as µCT imaging of the samples, the testing protocol and the analysis of anchor placement, followed by a look at the steps of data processing.

Chapter 5 covers the results of the conducted experiments, using characteristic variables to compare both groups.

In Chapter 6, the obtained results are discussed, limitations and possible future work are mentioned, and a conclusion is drawn.

Chapter 2

The Bone Tendon Interface

Active motion of the skeleton is caused by the contraction of muscles. In order to transfer muscular forces to the skeleton, a connection of high tensile strength is needed between muscle and bone. This is what the tendon is responsible for. The structures of bone and tendon both rely on different types of collagen, however, their mechanical properties differ.

This chapter will give an overview of the structure and composition of bone and tendon, as well as their interface, the enthesis.

2.1 Bone

2.1.1 Composition and Structure of Bone

Bone is the primary structural element of a mammal's body. It is essential for locomotion and is used for the protection of important organs.

In general, the components of bone can be split into organic and inorganic groups. The most abundant organic component is collagen. Collagen type I makes up 90% of all organic components in bone. Other organic components of bone are collagen types III, V, and XII, non-fibrous collagen, non-collagenous proteins (NCPs) as well as proteoglycans and lipids. The organic part of bone, especially the long collagen type I fibrils (Level 5-7), is responsible for high tensile strength. A water-NCP-matrix makes up a third of the total bone volume [10, 11].

Inorganic minerals, mostly represented by carbon-substituted hydroxyapatite, lead to the high compressive strength of bone. Together with other deposited minerals like sodium, potassium, or magnesium, minerals make up 62% of dry bone weight.

All those compounds are hierarchically structured. Starting from the highest level of a whole bone, the structure can be broken down into seven levels, as visualized in figure 1 [10, 12].

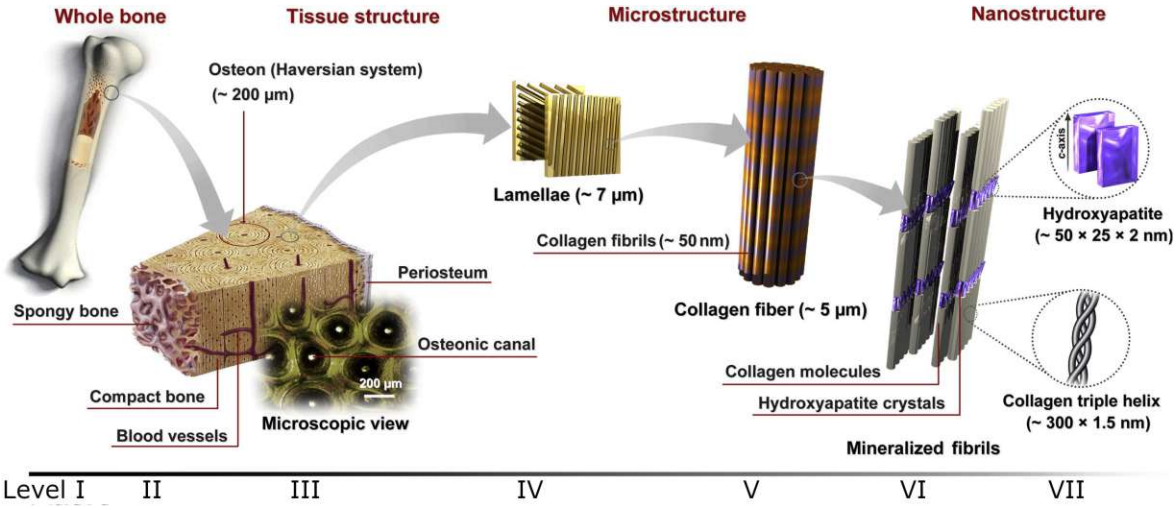

Figure 1: Schematic representation of the hierarchical structure of bone [13].

Level 1: Whole Bone

The shape and size of the whole bone (figure 1 I) are determined by its purpose. Tubular long bones like the femur and humerus are used as levers to induce motion, while flat bones like the skull can have protective functions. For this work, the bone of interest is the feline calcaneus, acting as the connection site between the foot and the calf muscles. It is classified as a short bone and its exact shape can be irregular.

Level 2: Cortical and Trabecular Bone Tissue

Depending on the purpose, some bones must withstand higher loads than others. The strength of a whole bone is influenced by its shape and its structure. An important macro-structural variable that influences strength is the porosity of bone tissue. While the goal generally is to be as strong as needed and as light as possible, bone can adapt its structure upon strain as shown in figure 1 II. Cortical bone is very dense and fracture-resistant, forming the outer layer of every bone. It makes up 80% of the skeletal mass. Spongeous trabecular bone is located in long and short bones, especially in the epiphysis and metaphysis. Also, tendon insertion sites show the presence of cancellous bone. Trabeculae (plates and rods) act as load-distributing material, avoiding stress concentration and minimizing weight. Apart from biomechanical properties, its main function is mineral homeostasis. Classification of cortical and trabecular is made by porosity, which is 5-10% in cortical bone and around 55-95% in cancellous trabecular bone [11, 14].

Level 3 & 4: Osteonal and Lamellar Structure

The compact material that makes up cortical and trabecular bone is arranged in different ways for both types. Under a microscope, cortical bone can be seen as an

arrangement of concentric units called osteons (figure 1 III). Each osteon consists of a central vascular channel, the Haversian canal, surrounded by layers of concentric lamellae. Osteons are bounded by cement lines rich in mineral and NCP density and low in collagen. Interstitial lamellae in spaces between osteons, as well as inner and outer circumferential lamellae at the boundaries of cortical bone, are also present. In order to increase torsional stability, the fiber direction of layered lamellae can vary within one osteon. The angle between fibers of adjacent units can be up to 90° with a maximal inclination of ± 45°as visualized in figure 1 IV.

Single trabeculae of cancellous bone have similar dimensions to a single osteon, however, they are structured in a different way. Trabeculae consist of trabecular packets - made out of lamellae - and interstitial lamellae, separated by cement lines. Trabecular bone has a high metabolic turnover rate and new trabeculae are arranged in direction of mechanical stress.

Both cancellous and cortical bone lamellae enclose lacunae and canaliculi, giving space to osteocytes and their interaction canals as shown in figure 2.

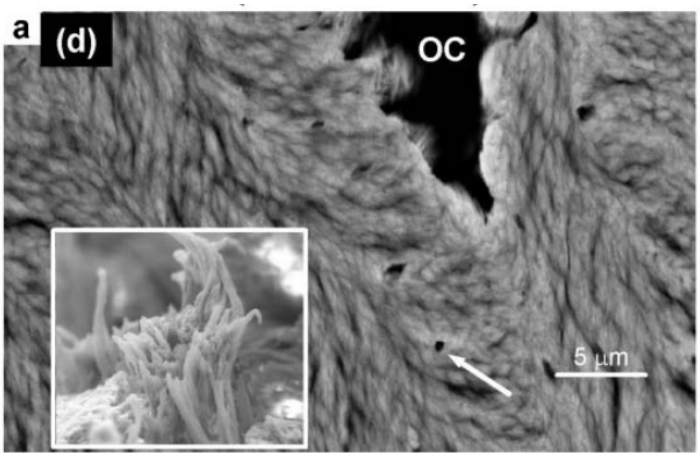

Figure 2: Lamellar and fibrillar texture surrounding an osteocyte lacuna (OC) as seen in scanning electron microscopy (white arrow). Insertion shows a bundle of mineralized collagen fibrils forming lamellae [15].

During growth or fracture healing, bone structure is described as woven bone. Instead of directional lamellae, collagen fibers occur in a more random arrangement. Biomechanically, woven bone is weaker and more flexible than lamellar bone [10, 11, 16, 17].

Level 5 - 7: Collagen Fibrils and Major Components

Lamellar units and woven bone both are made out of collagen fibers. A fiber with a diameter of about 5 µm is made of mineralized collagen fibrils, built by the periodic arrangement of tropocollagen. In figure 1 V, this periodic structure is highlighted. Different colors of the collagen fibril represent gap and overlap regions that form due

to the assembly of tropocollagen molecules. Mineral occurs both extra-fibrilar and intra-fibrilar using the space of gap regions of the collagen fibrils. The most important mineral is hydroxyapatite (figure 1 VI-VII). Mineralization and crystal growth are highly steered by NCPs. NCPs are located extra-fibrilar and are also responsible for adhesion between the organic and the inorganic components of bone [10, 11, 13].

2.1.2 Biomechanics of Bone

The field of mechanical properties of bone is well-researched. Due to the anisotropic and hierarchical structure of bone, biomechanical properties vary. Primarily, they depend on bone density, load type, and direction as well as possible pathological conditions [10, 18]. In general, the mechanical behavior of bone can not be seen as linear elastic per se. In order to compute characteristic values such as Young's modulus, linear elasticity is assumed in the following.

While cortical bone has a Young's modulus in the range of 17 and 27 GPa [19, 20] in the longitudinal direction, Young's modulus of trabecular bone is lower. Macroscopic tests of apparent compression show a Young's modulus of 200 - 600 MPa for trabecular bone [10, 18, 21]. Also, micromechanical and nanoindentation tests on trabecular bone suggest that its Young's modulus of 6.9 to 23.5 GPa [19] is lower compared to cortical bone. As visualized in figure 3, the apparent bone density is a very important factor for macromechanical tests. According to Frank et al. [22], lower apparent bone density due to osteoporosis does not lead to relevant changes in the material properties of individual trabeculae.

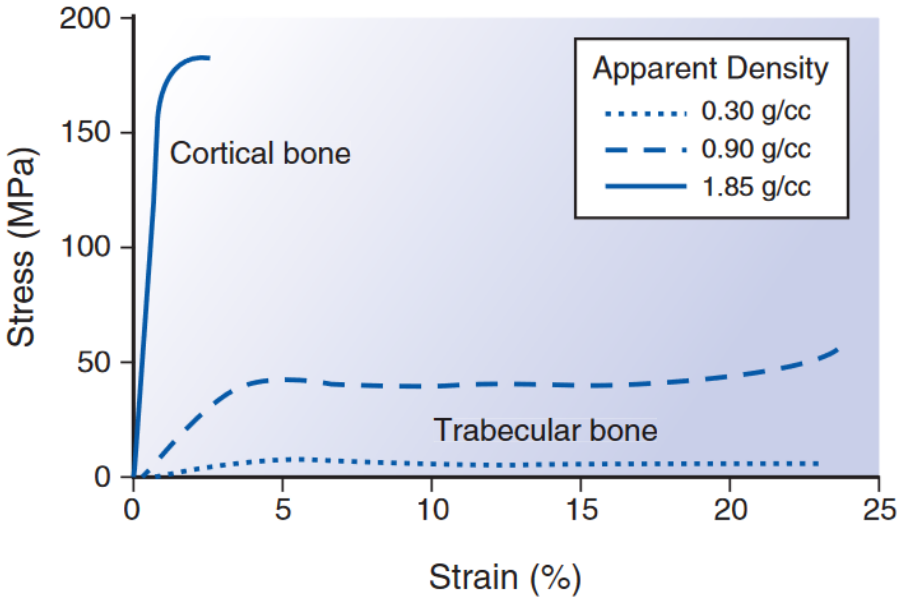

Figure 3: Stress-strain curve of cortical and trabecular bone [18].

Also, yield and ultimate strength depends on bone mineral density. The ultimate tensile strength of cortical bone is about 100 - 150 MPa [21]. While single trabeculae can reach similar values during micro-mechanical testing [19], the apparent ultimate strength ranges from 8 to 50 MPa. This is due to variations in density and direction of single trabeculae [10].

Even though other factors such as age, the load direction and loading rate can influence ultimate strength and Young's modulus [19], forces that occur in this study should be way below those thresholds and bone deformation or even failure is not expected. Instead, strain is expected to be observed at suture and tendon, leading to gap formation at the bone tendon interface.

2.2 Tendon

2.2.1 Composition and Structure of Tendon

The extracellular matrix of tendons is biochemically mainly composed of collagen, water, proteoglycans, and elastin. Similarly to bone, collagen type I is the structurally most important and also by far the most occurring type. The collagen fibers are aligned parallel to the tendon axis and are responsible for high tensile strength. Collagen types II, V, VIII, X, XI, and XII also occur in minor numbers and have different, mainly regulatory, roles. Proteoglycans are responsible for lubrication and hydration, enabling collagen to glide in the tissue matrix. The role of elastin is to restore the tendons' initial length after elongation due to loading.

This extracellular matrix is synthesized by fibroblasts, the so-called tenocytes. Mature tenocytes are located between collagen fibers and are characterized by an elongated shape along the direction of the tendon and a prominent nucleus.

Similarly to bone, the general structure of tendon can be described as hierarchical (figure 4). Sets of tropocollagen form microfibrils, grouped into fibrils and fibers. Units of tendon fascicles consist of collagen fibers and tenocytes and are surrounded by endotenon, a connective tissue enabling fascicles to glide independently.

Figure 4 also shows the crimped arrangement of collagen fibers, which enables tendon elongation in order to store energy and to smoothen load peaks for muscle protection [23, 16, 10].

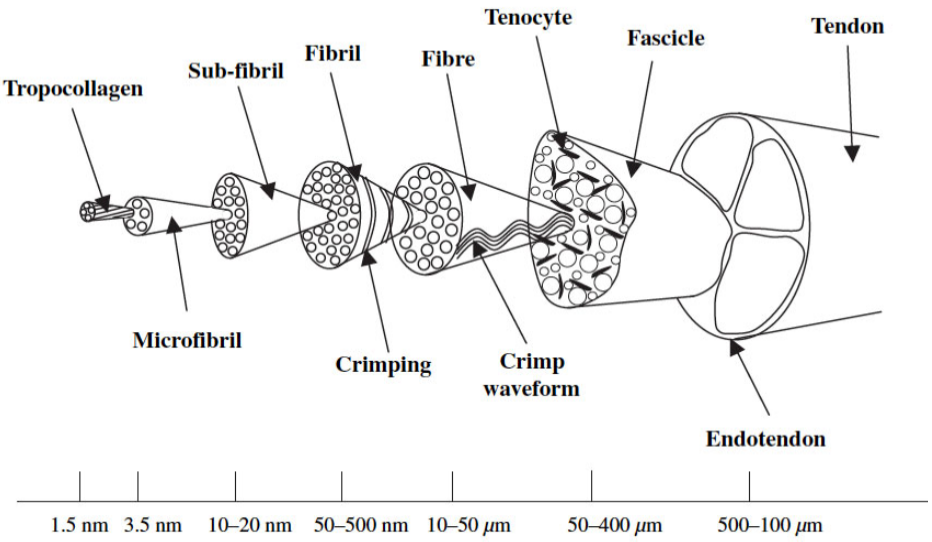

Figure 4: Schematic representation of the hierarchical Structure of tendon [23].

2.2.2 Biomechanics of Tendon

Due to the lack of mineralization compared to bone, tendons can only truly withstand a tensile load. Because this is the physiological type of load, uniaxial tensile testing of tendon material is of the biggest interest in research [16]. A general representation of those results is shown in figure 5.

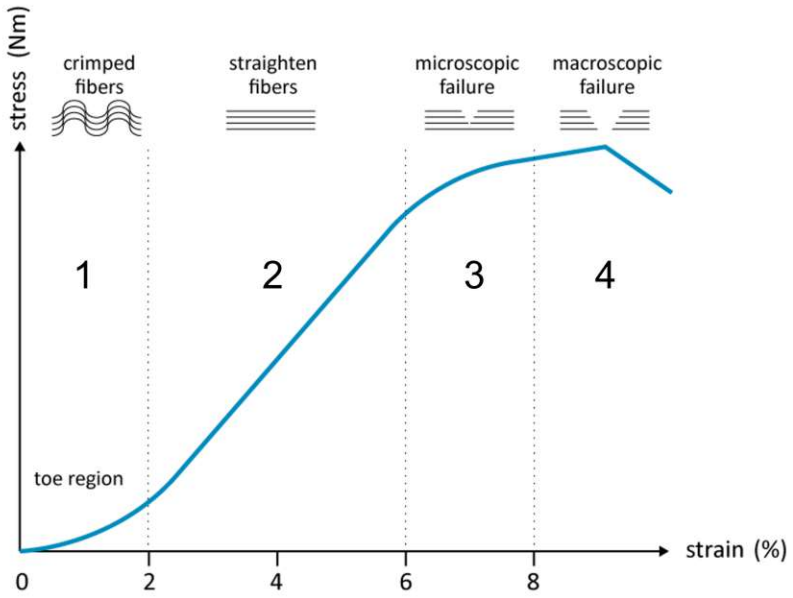

Figure 5: Typical stress-strain curve of a tendon, schematically divided into physiological (1-2) and pathological (3-4) regions [24].

The stress-strain curve can be parted into four regions. Up to a strain of about 1 to 3%, collagen fibers are still crimped. In this toe region, little load is needed to straighten out the crimped fibers. When fibers start to be straightened, the stress-

strain curve is seen to become almost linear in the second region. This behavior can be observed until the maximum physiological strain of about 6%. The maximum physiological strain can vary for different tendons and tendon locations and reaches up to 15%. In this almost linear elastic region, the initial length of the tendon can be restored and Young's modulus can be obtained by measuring the curve's slope. Here, values vary with different tendons, typical values for the linear region are 800 to 1200 MPa [10, 25]. The flattening of the curve in region three shows the beginning of pathological load. Microscopic damage leads to the tendon not being able to restore its initial length. Macroscopic damage, specifically a partial or complete tendon rupture can be identified in region 4. Also, ultimate strain values vary for different tendons. In general, the stress-strain curve depends on multiple variables of the experimental setup.

Viscoelastic properties of tendons generally describe the dissipation of energy in response to loading. Figure 6a shows hysteresis on the deformation-load curve of a tendon. The enclosed area represents energy that is lost due to viscous and viscoelastic behavior. Figures 6b and 6c respectively show relaxation and creep behaviour of tendon material [26, 10, 16].

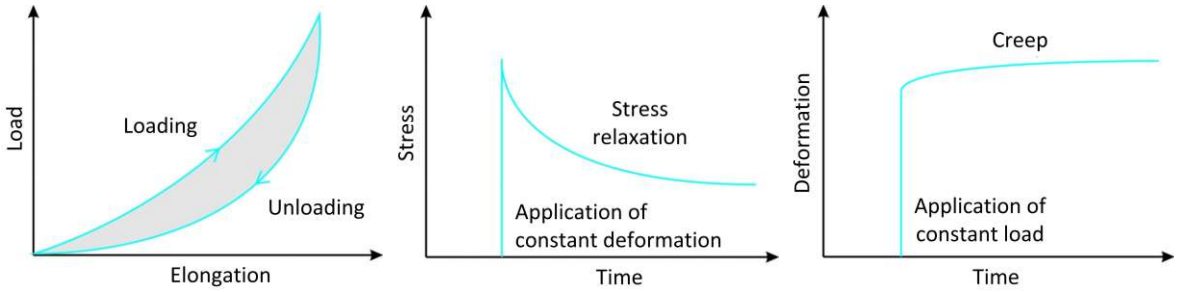

(a) (b) (c)

Figure 6: Viscoelastic characteristics of tendon: hysteresis (a), creep (b) and relaxation (c) as a response to load [26].

Relaxation is measured by maintaining a constant strain of the specimen and measuring the needed force or stress, which is observed to drop after the initial load. Vice versa, creep describes the elongation of a sample that is exposed to constant stress.

Those characteristics of viscoelasticity show, that consistent pre-conditioning of tested samples for any type of mechanical test is essential. Similarly, environmental variables like sample temperature and hydration influence the mechanical properties of tendon material [16].

2.3 Tendon Insertion

The insertion site of tendons, also called enthesis, is essential for load transmission between muscle and bone. In general, there are two different types of tendon and ligament insertions, called fibrocartilagenous and fibrous. In literature, they are also referred to as direct and indirect, or chondroapophyseal and perioesteal-diaphyseal [27, 28, 29]. Usually, the insertion type depends on its location at the bone. Tendon and ligament insertions at the epiphysis of long bones and to the tarsal short bones are fibrocartilagenous, while insertions to diaphysis and metaphysis are usually fibrous or indirect [30].

Indirect or fibrous entheses are directly connected to bone or periosteum. The dense connective tissue of mineralized collagen fibers perforates the bone at relatively large surface areas. Those perforating fibers are also called Sharpey's fibers. Exemplary for a fibrous tendon insertion is the human deltoid muscle, connected to the humerus shaft [29, 31].

Fibrocartilagenous entheses are more common at the most important tendon and ligament insertion sites and also most injuries induced by overuse are identified at direct tendon insertions. This may explain, why research has mostly focused on this type so far [27]. Typically, a direct tendon insertion can be divided into four zones, as shown in figure 7.

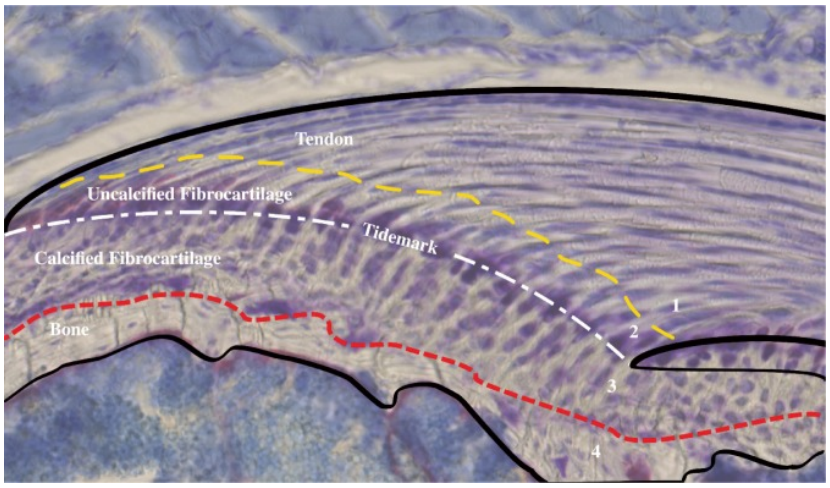

Figure 7: Histological section of a mouse supraspinatus tendon after staining of proteoglycans. Representation of four zones described for fibrocartilagenous entheses [29].

Dense Fibrous Connective Tissue

The zone of tendon consists mostly of type 1 collagen that is arranged in a parallel and linear way and fibroblasts, very similar to pure tendon. Hence, mechanical properties are very close "to those of mid-substance tendon" [29] as well.

Uncalcified Fibrocartilage

Uncalcified fibrocartilage is avascular and unmineralized. Collagen types I, II, and III, the proteoglycan aggrecan and fibrochondrocytes are present in this zone. The main function of uncalcified fibrocartilage is suggested to be the dampening of bending forces that act on collagen fibers. This theory is supported by the fact that more uncalcified fibrocartilage is present at tendon insertion sites with a higher variance of the tendon-to-bone angle [28, 29].

Tidemark

The border between uncalcified and calcified fibrocartilage can be identified in histological images as a relatively straight line, the tidemark. It acts as a mechanical boundary between soft and hard tissues. Collagen fibers that cross the tidemark, generally do so at a right angle [32].

Calcified fibrocartilage

The zone of true insertion of the tendon into bone is the zone of calcified fibrocartilage. Similarly to the previous zone, it is avascular and consists of aggrecan, fibrochondrocytes and collagen, however, collagen type II is dominant here and the zone is mineralized. Compared to the clear boundary of the tidemark, this zone is highly irregular. The interlocking nature of the boundary between uncalcified fibrocartilage and bone is important for the mechanical strength of the tendon insertion. Additionally, this zone acts as a barrier against vascularisation, cutting direct communication between bone and tendon cells [32, 28, 29].

Bone

The fourth zone of fibrocartilagenous tendon insertion is compact bone. Its structure is described earlier in chapter 2.1.

It is thought, that this transition between bone and tendon is supposed to "balance the different moduli of elasticity of the bone and the tendon" [32]. Observations in vitro and in vivo show, that the mechanical properties of healthy fibrocartilagenous tendon insertions are even stronger than bone. Overload by peak forces more often results in an avulsion fracture than in a damaged tendon insertion, however injuries due to overuse and repeated micro-trauma of direct entheses, often in combination with tendinopathy, are clinically relevant [27, 28, 29, 32, 33].

Chapter 3

Anatomy and Orthopedics of Feline Achilles Tendon Reconstruction

For the scope of this work, the investigated injury is the distal Achilles tendon rupture of the cat. A brief look at the anatomy and biomechanics of the feline hind leg complex will be followed by orthopedic reconstruction methods of tendon insertion. Last in this chapter, the concept of bioresorbable materials and implants will be discussed.

3.1 Feline Hind Leg Anatomy and Biomechanics

The anatomy of a feline hind leg is different from human ankles in various ways. Most importantly, as seen in figure 8, the calcaneus does not have contact with the ground. Musculus gastrocnemius and musculus soleus, together with their tendonous insertions to the calcaneus, keep the hind leg upright. Both muscles act parallel to the tibia with the muscular attachments respectively at the distal femur and the proximal fibula. Additionally, the superficial digital flexor muscle runs parallel.

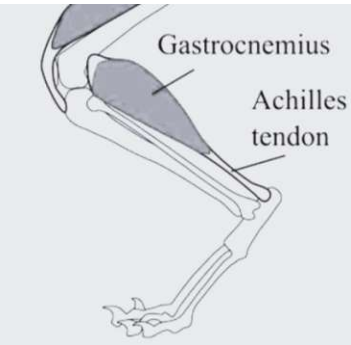

Figure 8: Representation of feline hind leg anatomy [34].

This upright position of the hind leg is present during the whole gait cycle, visualized in figure 9. Brown et al. [35] found out that during the stance phase, the tarsal angle (included by tarsus and tibia axis) ranges from 117° to 134°. Similar values were found

by Gregor et al. [36], with peaks of 147°. The experimental setup is designed to replicate this anatomical precondition, a tarsal angle of 125° is used.

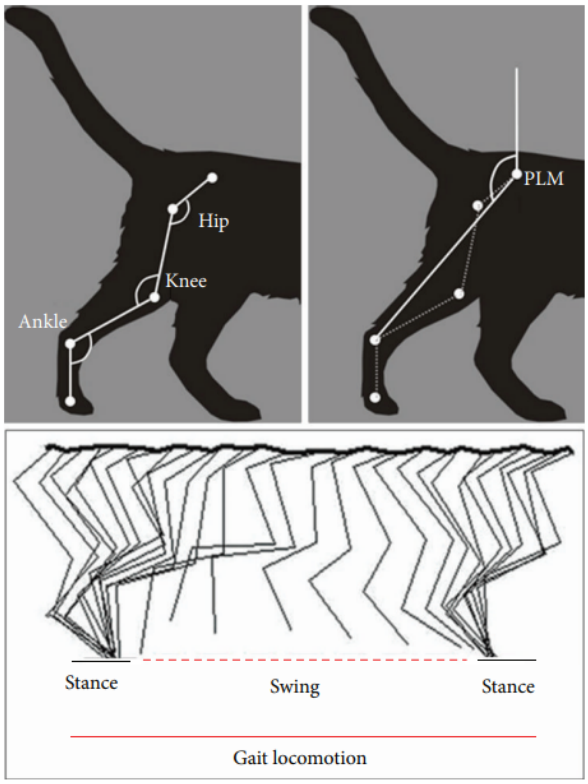

Figure 9: Representation of feline hind leg kinematics during the gait cycle [37].

3.2 Orthopedic Reconstruction Methods

Technology of tendon reconstruction methods has evolved both in human and veterinary medicine. Due to the focus on human applications, progress in veterinary use is slower. While intra-osseous tunnels for tendon re-fixation to bone are mostly replaced by specialized bone anchorage systems in human orthopedics, animals are still treated with the cheaper but sometimes more complicated tunnel sutures to a large extent. In the present case of a distal common Achilles tendon rupture, studies show that fixation of tendon directly to bone is biomechanically stronger than trying to use short distal tendon stumps for suture-only reattachment [38]. Montavon et al. [3] suggest the intra-osseous suture for feline Achilles tendon ruptures as the gold standard method. In addition, Scott et al. [39] suggest post-operative immobilization of the tarsal joint by the use of a lateral splint, an external skeletal fixator, or the placement of a calcaneotibial screw. Implanted fixations are to be removed after four weeks, the splint should be worn for a total of six to eight weeks after surgery [39, 3, 4, 40].

3.2.1 Suture Patterns

The clinical advantages and disadvantages of different suture techniques for tendon repair have been evaluated by many investigators in the past. Usually, biomechanical tests were conducted on tendon-tendon interfaces, and over time, state-of-the-art sutures were modified and have evolved constantly. Especially the idea of an earlier tendon mobilization after surgery, in order to reduce the risk of tendon adhesion, resulted in adaptions of Bunnell's technique first described in 1918 (figure 10) [41].

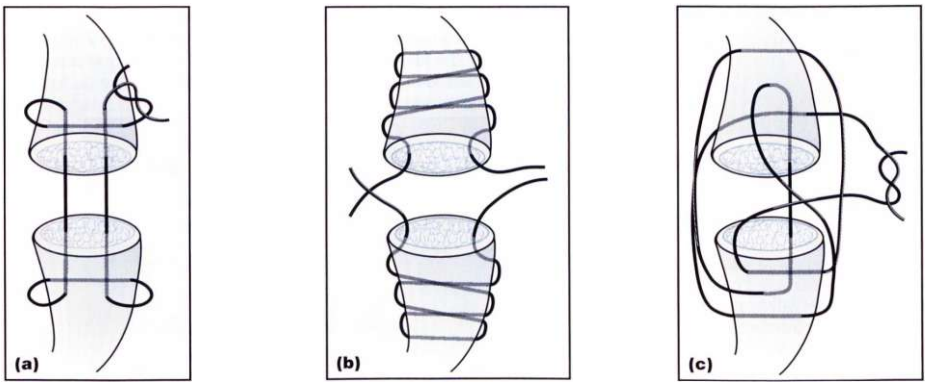

(a) (b) (c)

Figure 10: Suturing Techniques: (a) Locking Loop, (b) Bunnell-Mayer, (c) Three-Loop-Pulley [4].

Newer suture techniques started using multiple loops and strands to minimize suture gliding and gapping [42]. Studies show that multi-strand-sutures result in less gapping and higher ultimate strength, however the tissue damage due to additional stitches needs to be considered [43, 44, 45]. Figure 11a shows how general suture techniques compare in terms of mechanical performance, taking into account their complexity.

Here, the methods are split into three groups. Due to the hierarchical and unidirectional structure of the tendon, a simple strand of suture, perpendicular to the tendon's collagen fibers, would cut through the tendon upon load relatively easily. Instead, more advanced techniques use locking loops. As a response to load on the suture, the loop is tightened around a bundle of collagen fibers. This grasping mechanism, visualized in figure 11b, minimizes the problem of suture gliding [43].

For reattachment of feline Achilles tendon ruptures, simple suture techniques are commonly used. Montavon et al. [3] suggest a three-loop pulley suture, but also the Bunnell-Mayer suture is accepted. In the case of this study, only a one-sided suture is needed, as the suture is passed through a fixed tunnel or placed in the suture anchor in the calcaneus (Section 3.2.3) on the distal end of the ruptured tendon. Research shows that a fixed anchorage on one side significantly increases mechanical performance. In particular, it increases the force needed to pull a gap between tendon and anchorage, even with simple suture patterns [46]. For compatibility reasons with the Weldix®

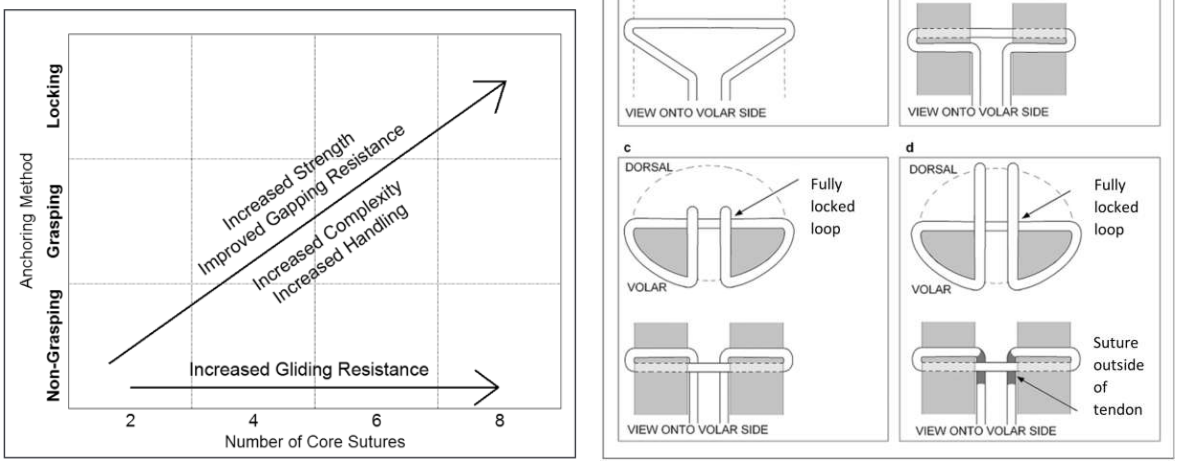

(a) Relationship between anchoring method and the number of core sutures [43].

(b) Locking principles in suturing techniques [43].

Figure 11: Suturing Principles

suture anchor [47], this study uses the Bunnell-Mayer suture technique for tendon repair. This method is currently also used in vivo in combination with the Vetwelding Weldix® anchor.

3.2.2 Intra-Osseous Suture

In the case of this study, the distal part, that the tendon of the control group is sutured to, is bone. There are different methods of fixing sutures to the bone. The simplest way is to drill a small tunnel into the calcaneus, the so-called intra-osseous suture tunnel. A suture is then threaded through this hole and both ends can be used to fixate the proximal tendon with one of the suturing techniques described earlier. For the feline Achilles tendon repair, this method is still suggested by Montavon et al. [3], Arthurs et al. [4], Scott et al. [39]. Here, the intra-osseous tunnel with a diameter of 1 mm is drilled mediolateral through the caudal calcaneus. Therefore, the bone needs to be accessible from both medial and lateral, and a considerable amount of tissue is affected during the operation. Overall this procedure is relatively time-consuming [5]. Figure 12 shows the µCT image of an intra-osseous tunnel in the feline calcaneus.

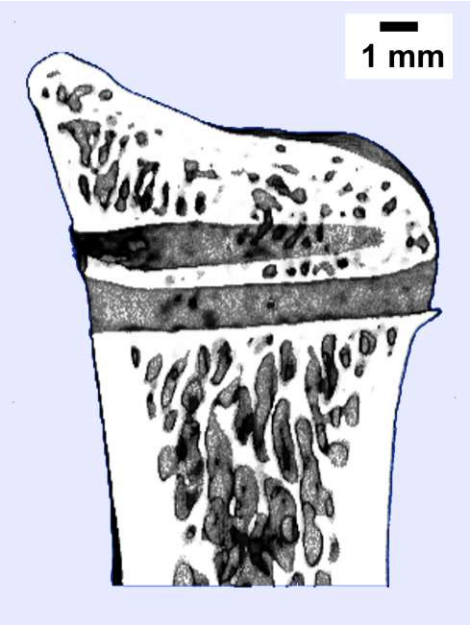

Figure 12: µCT-Image of an intra-osseous tunnel for the repair of the feline Achilles tendon.

3.2.3 Anchor Implants

A more modern alternative method of fixing suture to bone is the use of suture anchors, i.e. bone implants that can be loaded with the desired type of suture and holding them in place. The tendon, or soft tissue in general, is fixed to the anchor's sutures similarly to the intra-osseous tunnel technique, using the suturing techniques described in section 3.2.1. Studies suggest that suture anchors might yield biomechanically better results compared to intra-osseous sutures [48]. Principles of anchor implantation vary and new methods are developed constantly [49]. Differences also occur in anchor shape and material resulting in different biological interactions with bone tissue. The following principles are used in human and veterinary orthopedics today, depending on their application and the preference of the surgeon. An overview is given in figure 13, where different suture anchor shapes and principles are shown.

After the description of different fixation principles, material options and choices will be explained.

Threaded Anchors

Before more sophisticated suture anchors were available, a similar technique was applied by pressing a suture to bone by using simple bone screws and washers. One of the first commercially available suture anchors was patented by Goble et al. [52] in 1995. It is a self-drilling, threaded hex screw made of titanium with an attached suture. Other than earlier anchor systems using simple bone screws, the suture was here embedded into the screw underneath the bone surface, suture orientation is optimized

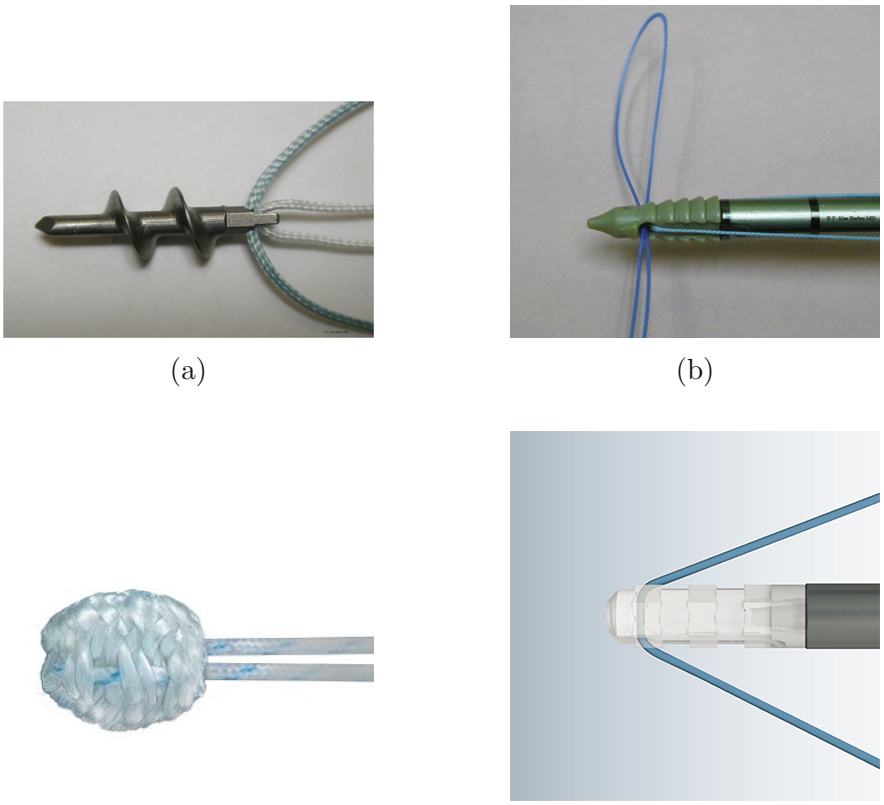

(a) (b)

(c) (d)

Figure 13: Suture anchor fixation types: (a) Threaded anchor [50], (b) Push-in anchor [43], (c) All-suture anchor [51], (d) VetWelding Weldix® [47].

and slippage of the suture is eliminated. Modern threaded anchorage systems such as the Arthrex Corcscrew©, which is shown in figure 13a, have optimized the thread shapes and materials for cortical or cancellous bone fixation and are commonly used for several applications. They are relatively easy to use and well-proven. A disadvantage is the result of bone stress upon implantation. Especially small bones, such as the feline calcaneus, require stress-free implantation to reduce the risk of bone damage.

Pressfit Anchors

Alternatively, anchors are pressed into pre-drilled holes with force. Here, the diameter of the anchor is larger than the hole, which leads to a press fit. Exemplary, the ConMed PressFT™ anchor is shown in figure 13b. Compared to threaded systems, press-fit anchors can have smaller outer diameters and are easier to implant. However, these anchors often are designed with the suture being pressed between the anchor body and bone. This may lead to suture cutting through bone as Ono et al. [53] suggest. In general, pull-out forces are lower compared to screw-in suture anchors [5].

All-Suture Anchors

The use of all-suture anchors is relatively new and little research has been performed on them. First studies are not very consistent in terms of anchor stability, with some studies suggesting similar results to traditional anchors [54, 55] and some observing inferior mechanical performance and early anchor displacement [56]. A big advantage of all-suture anchors is the smaller size compared to solid anchors, as seen in figure 13c. It can be applied in places, where traditional anchors are too large and can not be implanted. In addition, the soft suture material is more gentle to bone material compared to rigid polymer implants mentioned above, resulting in less bone damage during implantation and a lower risk of joint damage in case of anchor failure [5, 56]. There is no specific literature on the use of all-suture anchors in veterinary medicine, however small animal applications might be interesting in the future, as anchor dimensions would be suitable for small animal applications. For the application of the repair of a ruptured feline Achilles tendon, the lack of selection of suture sizes makes the all-suture anchor unsuitable for now.

VetWelding Weldix® anchor

A new approach to anchor placement is the BoneWelding® technology. Here, a hole is pre-drilled into bone, similar to pressfit anchor systems. The anchor, made of thermoplastic Polylactide, is implanted into the hole, while being heated via ultrasonic vibration, similar to pressfit anchor systems. This vibration liquefies small amounts of the polymer due to shear forces at the anchor-bone interface and enables the material to penetrate trabecular tissue structure [7]. This form-fit between bone and anchor leads to high pull-out forces as the company visualizes in figure 14. these internal tests were conducted in blocks of artificial bone (Cellular Rigid, 20pcf, Sawbones©, USA). Implantation and testing was performed hydrated at a temperature of 37 °C.

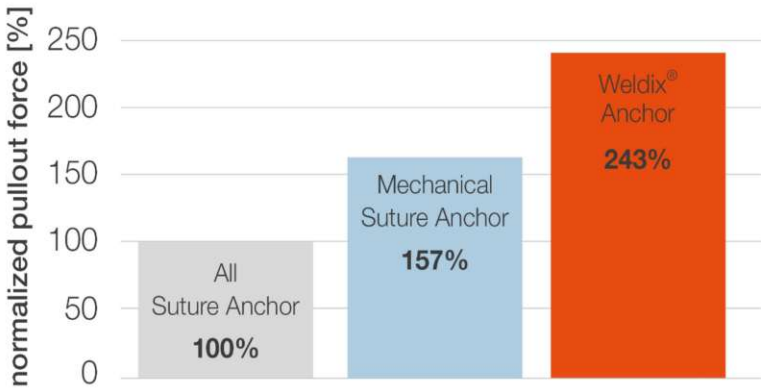

Figure 14: Pullout forces of different anchor systems from Sawbone, normalized to all-suture anchorage. [47].

Biomechanical tests by Güleçyüz et al. [57] show, that the SportWelding® Sombrero - used in human orthopedics - performs similarly to the larger screw-in anchor system. First clinical tests of the BoneWelding® Fiji® anchor, the direct equivalent to the VetWelding anchor for human orthopedics, show promising results for the therapy of Stener lesions of the thumb [58].

In veterinary medicine, the VetWelding Weldix® suture anchor (figure 13d) is applied for several procedures, including the repair of the feline Achilles tendon. Due to its small dimensions with a diameter of 2.3 mm (the drilled hole has a diameter of 1.8 mm) and a length of 7.2 mm, it can be used in places where minimal bone material is available.

Anchor Materials - Bioresorbability

Depending on their application, suture anchors are made of different materials. Most self-drilling anchors are made of titanium. Its good biocompatibility with minimal inflammatory response compared to other metals like stainless steel is the reason for titanium being used in a broad variety of medical implants. However, disadvantages such as loosening, cartilage damage, or imaging interference have accelerated research on anchors made of polymers. Depending on the application, these usually consist of long-chain macromolecules built by monomers, interconnected with covalent bonds [59, 60]. Non-metallic anchor materials can be grouped by their bioresorbability. Biodegradable polymers were used in orthopedics since the 1970s when the first biodegradable sutures made out of Polyglycolic acid (PGA) were introduced. The use of PGA for suture anchors was suspended due to the materials' fast degradation, starting only one week after implantation. The observed complications included anchor failure and inflammation as a response to degradation products [59]. The slower biodegradation of poly-lactic acid (PLA), along with its good biocompatibility, was found to be a promising alternative. Degradation times of up to five years have shown to be too long and were hindering complete replacement by bone material [59]. In order to control degradation time, different co-polymers can be added.

To eliminate the problems of biodegradable anchors, implants made of biostable polymer were introduced. Especially Polyetheretherketone (PEEK) is widely used because of its high mechanical strength and high resistance against heat and wear [59]. The big disadvantage of PEEK is its low potential for osseointegration. Manufacturers try to avoid this problem by coating the implant with more bioactive polymers or bioceramic material like hydroxyapatite [61].

Apart from coatings, another way of combining the advantages of different materials is the use of biocomposites, mixtures of resorbable polymers, and a bioceramic material that has osteoconductive and strengthening properties. Ceramics used for biocomposites are beta-tricalcium phosphate (β-TCP), hydroxyapatite, calcium sul-

fate, and calcium carbonate [59, 62]. A similar mineral composition to bone, as well as the micro- and macro-porosity, are responsible for the ceramics' stimulative properties. Especially β-TCP is known for its high osteoconductivity, making it a common material used for biocomposite suture anchors [59].

The material choice for the use of suture anchors is ideally individually chosen for every application. The expected duration of healing, mechanical requirements and bone quality play a role in this decision [59].

Chapter 4

Materials and Methods

The aim of this study is to compare the behavior of two different methods for feline Achilles tendon repair, the intra-osseous tunnel suture, and the VetWelding Weldix® suture anchor. To ensure a reproducible procedure, several steps need to be followed. In figure 15, all steps of the experiment are visualized. Sample harvesting and preparation was conducted at a veterinary clinic (Tierklinik Sattledt, Austria), represented in red below. In the following, all steps are described in detail, chronologically as occured in the project.

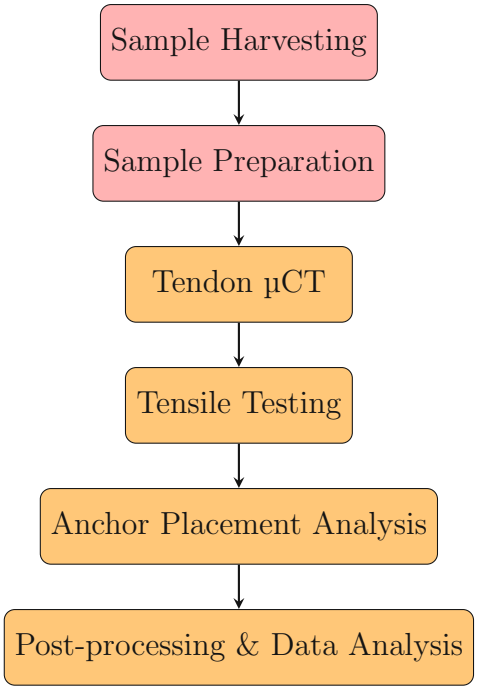

Figure 15: Representation of all steps during preparation, experimental testing and data analysis

4.1 Sample Harvesting and Preparation

For this study, seven pairs of feline calcanei with the attached Achilles tendon and calf muscles were tested. The samples were harvested from fresh frozen cat cadavers by a trained veterinarian. Only cadavers with two healthy ankles were used. One ankle was later prepared by intra-osseous suture and the contra-lateral by suture anchor. By using paired samples, variance due to anatomical preconditions between both preparation methods was expected to be reduced. The age of donors may vary and was not known for all cadavers used in this study.

For sample preparation, any additional soft tissue present at the bone-tendon interface was removed in order to eliminate tissue obscuring the camera view during the experiment. The gastrocnemius and soleus tendon were dissected together from the calcaneus using a scalpel, simulating a torn Achilles tendon, close to the tendon insertion site. Remaining soft tissue and tendon residues were removed from the bone to obtain a clean surface. To ease bone fixation later in the experiment, prominent processes of the distal calcaneus were removed. The calf muscles were shortened on the proximal end and the tendon was again cleaned from any soft tissue, before starting with re-fixation.

Intra-Osseous Suture

The tendon re-fixation procedure by intra-osseous suture is performed on one sample of every harvested pair, these samples were used as a control group. The procedure described in section 3.2.2 is used, with the tunnel being drilled before tendon dissection. By doing so, the correct mediolateral orientation of the tunnel can be ensured. Figure 16a shows the drill and calcaneus after drilling the mediolateral tunnel. The drill used for this procedure has a diameter of 1 mm. A Prolene suture (Optilene 2/0, B. Braun, Melsungen, Germany) is used to re-connect bone and tendon, applying the modified Bunnell-Mayer suturing technique. Therefore, the suture needs to be wrapped around the proximal calcaneus. The fully repaired sample is shown in figure 16b.

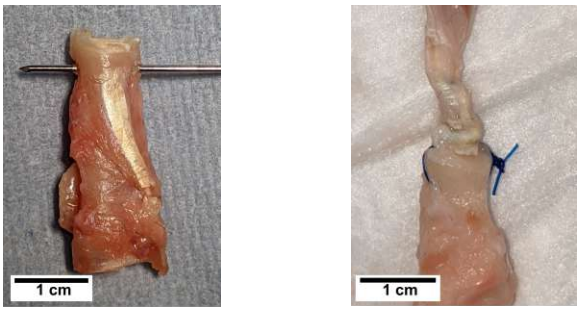

(a) (b)

Figure 16: (a) Intra-osseous tunnel, (b) Completed intra-osseous tunnel repair.

Weldix® Suture Anchor

For reconstruction with the VetWelding Weldix® suture anchor, a hole is pre-drilled using the VetWelding Weldix® Twist drill. Drill and drilling process are shown in figure 17a and 17b.

(a)

(b)

Figure 17: (a) VetWelding Weldix® Twist Drill [47], (b) Drilling process.

The conical shape on top of the drill is supposed to bridge over from cortical to trabecular bone. After drilling, the implantation process with the BoneWelder Vet ultrasonic generator can proceed as visualized in figure 18. Here, a Weldix® anchor is loaded with the same suture as used for the intra-osseous suture (Optilene 2/0, B. Braun, Melsungen, Germany).

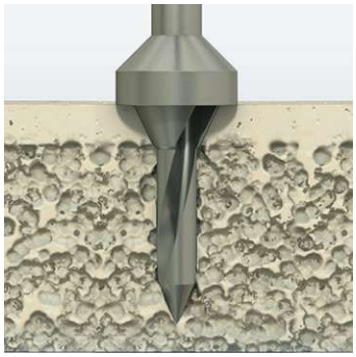

(a)

(b)

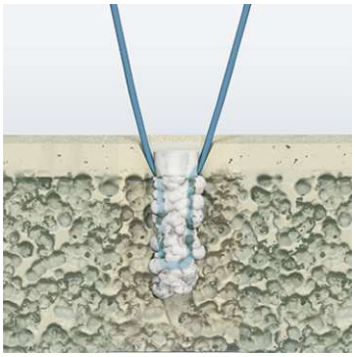

(c)

Figure 18: (a) Pre-drilled hole [7], (b) Implantation process using the BoneWelder® Vet ultrasonic generator , (c) Successfully implanted anchor [7].

Using both ends of the suture, the Achilles tendon is subsequently sutured to the bone using the Bunnell-Mayer technique. In comparison to the tunnel suture, less suture material is threaded through the bone anchor. Other than after intra-osseous tunnel preparation, the orientation of both suture ends is already in line with the tendon. After preparation, samples are wrapped in gauze and drenched in Hanks' Balanced Salts Solution (HBSS, pH = 7.4) in order to simulate physiological conditions. For transport and until testing, they were frozen at a temperature of -20 °C.

4.2 µCT Imaging - Tendon

On the testing day, the samples are thawed to room temperature in an HBSS bath. Before mechanical testing, information on every sample's geometry is obtained by µCT imaging (µCT 100, Scanco Medical, Brüttisellen). To calculate tendon stress during testing, the cross-sectional area of the tendon is needed. Despite µCT generally being used for imaging of mineralized tissues like bone, the bare tendon - surrounded not with any other soft tissue but air - can be made visible. To enhance image quality of the tendon, a low voltage of 45 kV is used, combined with a tube current of 200 µA.

For imaging, the prepared sample was placed in a styrofoam mold as seen in figure 19a, made to minimize strain on the sample during imaging. The cylindrical sample holder (figure 19b) is closed air-tight to eliminate drying of samples before testing.

(a) (b)

Figure 19: (a) Styrofoam mold, (b) Sample holder setup.

For image processing, the software medtool (medtool 4.5, Dr. Pahr Ingenieurs e.U., Austria) is used. By applying a gray value threshold, the sample is segmented from background, i.e. the styrofoam mold, and binarized. Selection of a region of interest (ROI) was done in a standardized way by enclosing the tendon into a box starting from the most proximal part of the calcaneus until the highest strand of suture seen in the tendon. The box is oriented along the tendon's length axis. Figure 20a exemplary shows ROI selection. In figure 20b, the resulting binarized ROI after image processing via medtool can be seen.

An average cross-sectional area is calculated as in formula 1:

$$CS_{\text{average}} = \frac{Volume_{\text{tendon}}}{Length_{\text{box}}} \tag{1}$$

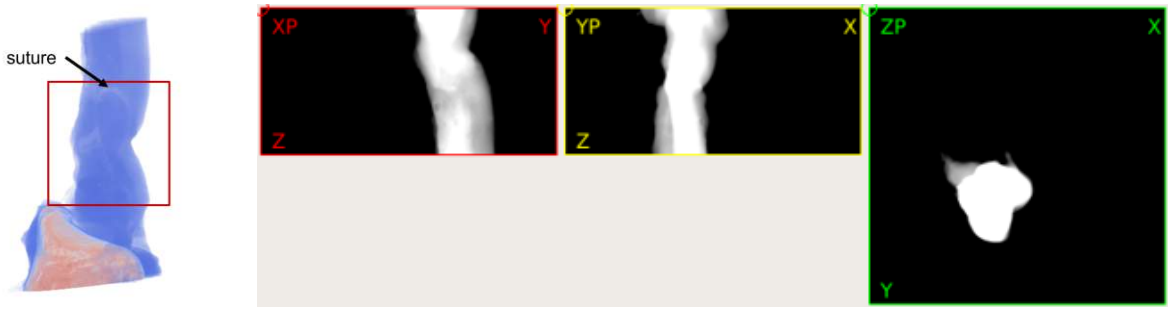

(a) (b)

Figure 20: (a) Selection of a region of interest for tendon cross-sectional area by limiting the box with the calcaneus and the highest strand of suture, (b) ROI after processing via medtool.

4.3 Biomechanical Testing Setup

The aim of the overall experimental setup is the replication of physiological load on the repaired Achilles tendon. To do so, the general setup principle including a sample fixation and the tensile testing machine is developed (figure 21).

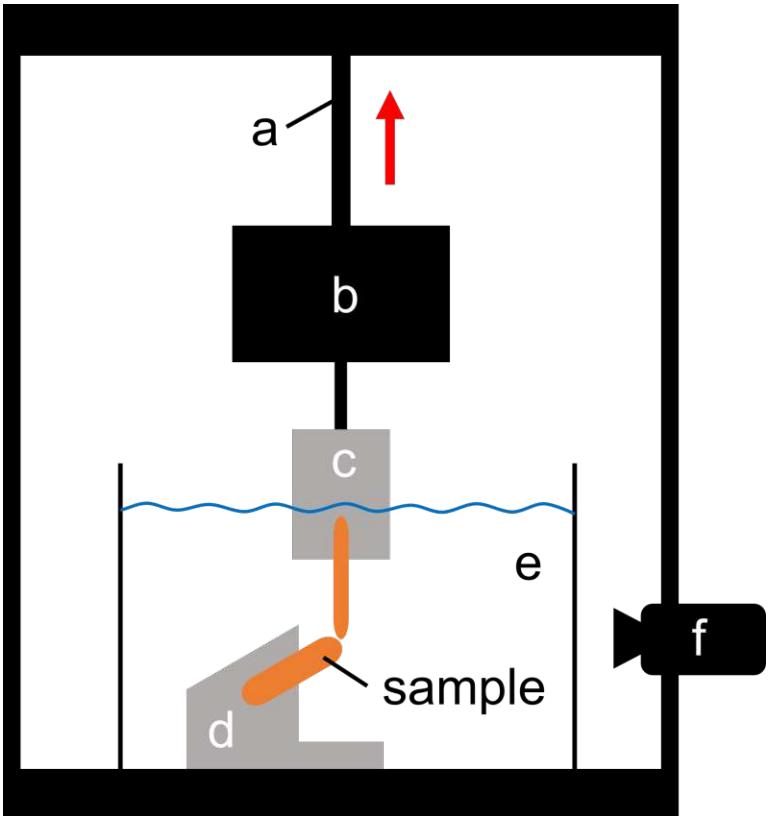

Figure 21: Experimental setup principle for biomechanical testing of repaired feline Achilles tendon samples. a: electromechanical actuator of tensile testing machine, b: load cell, c: tendon clamp, d: bone clamp, e: HBSS bath, f: camera.

For calcaneus fixation, two blocks of stainless steel are manufactured in a way that

allows the bone to be placed and wedged into a groove (figure 22a). When placed in the setup, the calcaneus is positioned at an angle of 125° with respect to the vertical axis. The bone fixation is screwed to the bottom of the tensile testing machine in a way, that the bone-tendon interface is exactly below the actuator. This ensures a physiological load direction.

A tendon fixation is developed similarly to Shi et al. [63] and Jiang et al. [64]. Two outer aluminum plates and two inserts, shown in figure 22b can be tightened by four screws and wedge the tendon in place. Grooves that are milled into the inserts make sure that no tendon slippage occurs during testing. A screw, mounted through both outer plates (figure 22c), acts as an anchor point. Using a hook, the sample fixation components are connected to the load cell (S2M/100N, HBM Germany), which is screwed onto the tensile testing machine, a servo-electric load-frame (Thelkin SELmini-001, Theklin AG, Switzerland).

(a) (b) (c)

Figure 22: (a) Bone fixation for physiological bone placement: 125° between bone and vertical axis, (b) Tendon clamp: insertions, (c) Tendon clamp: assembled.

A video camera (KITMOCAM 5M, Kiotech, Meckenheim) is placed perpendicular to the tendon and at the height of the bone tendon interface. Both proximal calcaneus and distal tendon are in the field of view. In order to create background contrast, black fabric is placed behind the testing setup. Camera recording is acquired via software (OBS Studio 27.0.1) with a magnification of 0.7 at a frame rate of 10 fps. Lighting is optimized individually for every sample using adjustable lights.

4.4 Testing Protocol

Before placing the sample in the experimental setup, the load cell is zeroed while holding the weight of the fully assembled tendon clamp. Next, the sample is fixed to bone and tendon fixation without applying tension on the tendon as visualized in figure 21. For tendon preconditioning, and to allow a consistent starting point for all samples, a tensile load of 1 N is automatically approached by moving the actuator

upwards. This method is in line with similar studies [65, 46, 66, 67, 68]. After reaching the desired tension, a pause of 5 minutes allows for tendon relaxation.

Displacement of the tendon clamp is driven with a constant velocity of 20 mm/min, similar to studies of Jordan et al. [46], Putterman et al. [67], Dunlap et al. [69] and Cocca et al. [68]. The displacement profile was programmed using software of the mechanical testing device and is shown in figure 23. Detailed settings for within the software are the constants $K_{\mathrm{pp}} = 1,5$, $K_{\mathrm{pv}} = 1,5$, and the time interval $T_{\mathrm{iv}} = 12ms$. Those constants are control parameters, used to calculate a reference and actual voltage for the positioning of the actuator during every time interval $T_{\mathrm{iv}}s$, ensuring accurate displacement.

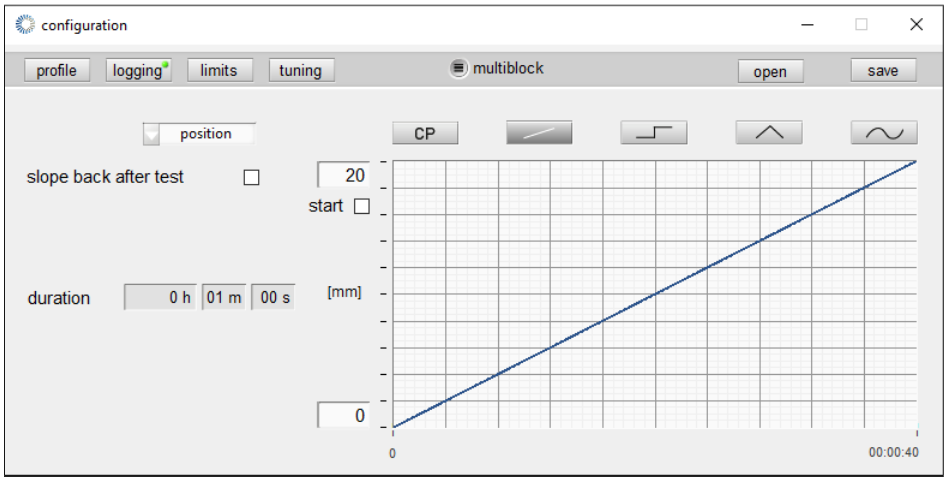

Figure 23: Displacement profile with constant velocity for mechanical testing of tendon sample.

The displacement-controlled setting chosen for this setup requires displacement and time as input variables in order to create a constant displacement velocity. The values are chosen depending on the available space for the tensile testing machine to pull, which is limited due to the frame size of the machine. If possible, a displacement of 20 mm over 60 seconds is chosen. If less than 20 mm were available, displacement of 18 mm over 54 seconds or 16 mm over 48 seconds are chosen. In all measurements, those values were enough to either create a sufficient gap between bone and tendon or lead to suture failure. During testing, the load is measured by the load cell with a frequency of 10 Hz, in line with the video frame rate.

4.5 Analysis of Anchor Placement

After testing, tendon and suture are dissected from bone. Anchor samples are further examined for anchor placement. Therefore, a µCT image of bone and anchor is made and the bone porosity in the area of anchor placement is determined. High or low bone density may indicate bad or good anchor placement, as anchor material is supposed to penetrate porous structures of the calcaneus. Steps for porosity determination are shown in figures 24 and 25.

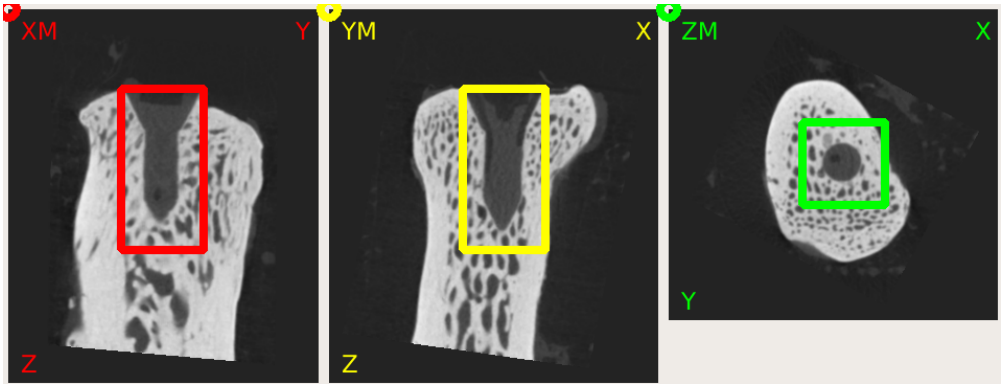

Figure 24: ROI selection on the rotated µCT image.

(a) Selected ROI (b) Mask (c) Segmented Bone

Figure 25: Steps of porosity determination.

First, the image is rotated in a way that the anchor length axis is parallel to the vertical image axis. From here, ROI selection can be done in a standardized way. As the drill and anchor cross-sectional area is equal for all samples, the cuboid ROI has the same dimensions for every image. While the anchor has a diameter of 2.3 mm, ROI has dimensions of 4x4 mm. By automatically filling all pores enclosed by bone, a bone mask is created and the total volume of bone in the ROI is calculated. By binarizing volume inside this masked ROI, every voxel is identified either as compact bone or background. By applying formula 2, bone porosity in the anchor region is calculated.

$$Porosity = 1 - \frac{Volume_{\text{bone}}}{Volume_{\text{mask}}} \tag{2}$$

After µCT imaging for estimation of bone porosity, all bones that were prepared by anchor are cut in half. Cuts are made in the sagittal plane and as central as possible through the anchor (figure 26a) using a low-speed saw (IsoMet Low Speed Precision Cutter, Buehler). Looking at the cut surfaces under a microscope, as shown in figure 26b, the molding behavior of the anchor can be observed retrospectively. Along with porosity, those evaluations are later checked for possible correlation with suture failure force.

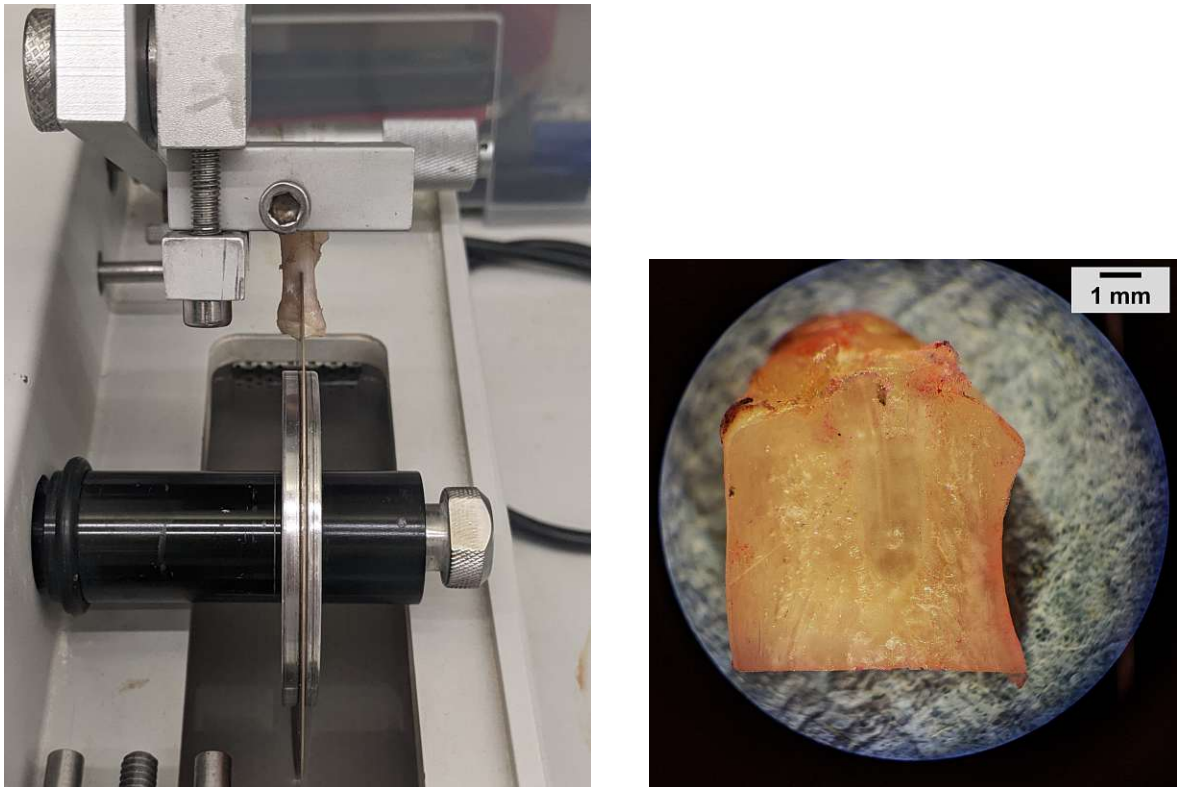

(a) (b)

Figure 26: (a) Setup for cutting using the Buehler Low Speed saw, (b) Cross section of halved bone, as viewed through an optical microscope.

4.6 Data Processing

Raw data is processed by self-developed programs. Before starting the analysis, video and load files are synchronized. Video frames are manually examined one by one and the last frame before motion is detected is used as a starting point, as it matches the first entry in the load file. Because of the same sampling frequency of 10 Hz, the number of video frames is supposed to be equal to the number of load file entries. The video data is cropped accordingly, using starting point and measurement duration.

4.6.1 Gap

Gap detection is done semi-automatically, using an self-developed Python program based on OpenCV contour detection. It analyses frame by frame and returns average gap values in mm.

Starting the analysis, gaussian filters are applied to smoothen bone and tendon edges in the image and get rid of small soft tissue artifacts. The region of interest (ROI) that is supposed to be checked for gap formation, has to be selected by user input as in figure 27. The region is supposed to only include bone and tendon and no background. This area is the starting point for further image processing.

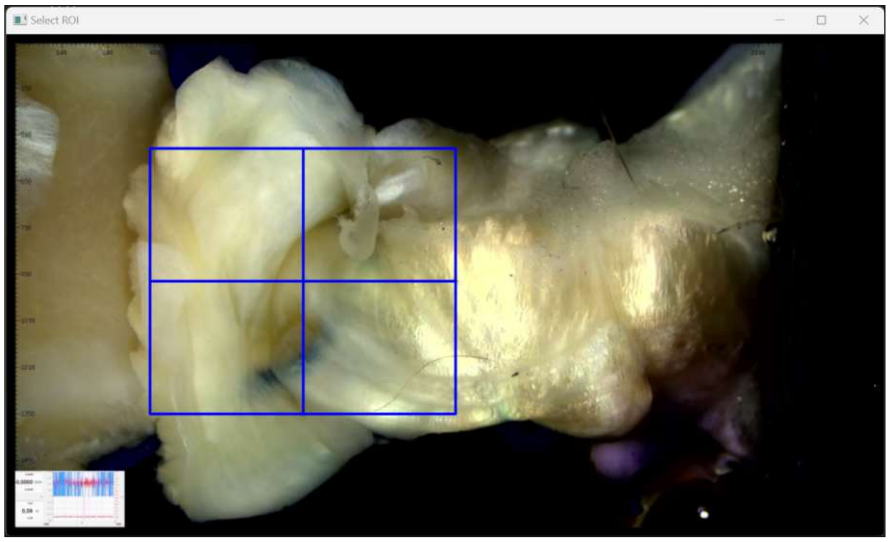

Figure 27: ROI selection via user input for gap detection.

A threshold is selected to binarize the original frame that is shown in figure 28a. The goal is to segment background - that is later registered as the gap - from bone and tendon. The threshold value needs to be individually chosen for each sample, as lighting conditions and sample color can vary. Binarizing leads to an image as shown in figure 28b, depicting bone or tendon in white and background in black. Using the Python library OpenCV, a contour-detecting algorithm is applied to the selected and binarized ROI. In particular, big contours of white bone or tendon are computed here. Results of this contour detection are used for re-iteration of the ROI that was given as user input, based on two possibilities depending on the observed frame:

1. mode: One contour is found - no gap or only a partial gap between bone and tendon

2. mode: Two contours are found - bone and tendon are completely separated

From the start, the program uses mode 1, as there is no gap between bone and tendon at all. As long as there is no complete gap between bone and tendon, every frame is cropped to the user input ROI, which is further processed. Once a full

separation between bone and tendon is registered, the upper and lateral ROI bounds are re-calculated for every frame with the intention to follow the path of the tendon horizontally and vertically.

After the ROI is determined, another contour-detecting algorithm is applied. Now, the contours of the black background are computed by inverting the image. Small artifacts (e.g. shadows, stains on bone and tendon or suture) can be removed by assigning a minimal contour surface area that is found by the algorithm. A resulting contour of this step is shown in figure 28c. It has to be noted that in the case of a partial gap, more than one gap contour can be found.

The accumulated area of all background contours in the ROI is returned. The mean gap between bone and tendon is calculated using formula 3:

$$Gap_{\text{average}} = \frac{Area_{\text{background}}}{Width_{\text{ROI}}} \tag{3}$$

The resulting value for the mean gap is written onto the image that is shown during data analysis (figure 28d) and written to a text file.

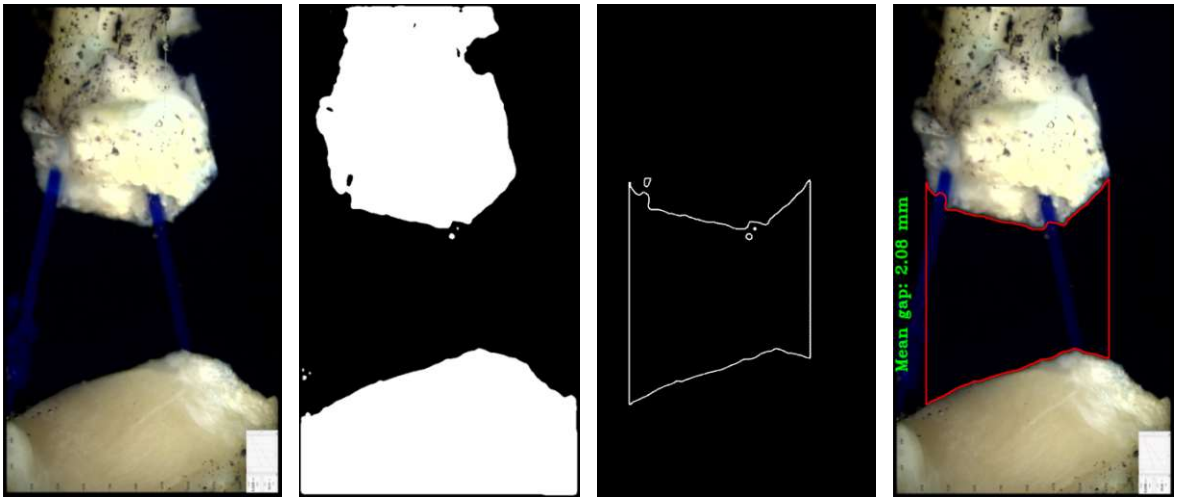

(a) Raw image (b) Binarized image (c) Gap contour (d) Visualization

Figure 28: Steps of image processing for gap detection.

4.6.2 Result Selection

Once gap formation is evaluated, both gap and load files are analyzed and visualized using Matlab (R21b, MathWorks, Natick, USA). After checking for correct synchronization, characteristic values based on similar studies are calculated [8, 65]:

- Load at 0.5 mm / 1 mm / 3 mm Gap
- Stress at 0.5 mm / 1 mm / 3 mm Gap
- Gap at 30 N Load
- Gap at 45 N Load
- Failure Load

While Moores et al. [8] focus on the load at 1 mm and 3 mm gap in their study on canine tendons, those values seemed high for this application. To scale characteristic values down, the 0.5 mm gap was added, as well as stress for consideration of geometrical circumstances.

Bone porosity is checked for correlation with failure load, as the micro-structure of bone can influence the proper implantation of the anchor. Bad implantation can lead to suture damage, resulting in early suture failure.

4.6.3 Statistics

The goal of this experiment was to pairwise compare the results between intra-osseous suture and suture anchor. However, was found that results are not always suitable for pairwise comparison. For example, a gap of 1 mm was only reached in both groups in 3 pairs. A 3 mm gap was only reached using the intra-osseous suture, resulting in no pair at all. The decision was made to use a pairwise test only if a minimum of 5 pairs are available. This was the case for:

- Load at 0.5 mm Gap
- Gap at 45 N Load
- Failure Load

In particular, a paired t-test was conducted on those results. In order to include all results, there was also an independent t-test applied to those results.

All other results from section 4.6.2 were treated solely as independent variables. The F-test was applied to check for equal variances. In case they were equal, an independent t-test was used. If the variances were unequal, Welch's t-test was applied.

All statistical tests were conducted two-sided. For all tests, a level of significance of $\alpha = 0.05$ was used.

To compute a possible correlation between bone porosity and failure load - only within the group of suture anchors - the Pearson correlation coefficient was calculated. All statistical analysis was computed using SPSS Statistics (IBM, Armonk, USA).

Chapter 5

Results

5.1 Load & Gap Measurement

As an example, figures 29a and 29b show the complete results of load and gap measurement of a pair of samples during testing. For clarity, plots of all other tested samples are attached in Appendix A.

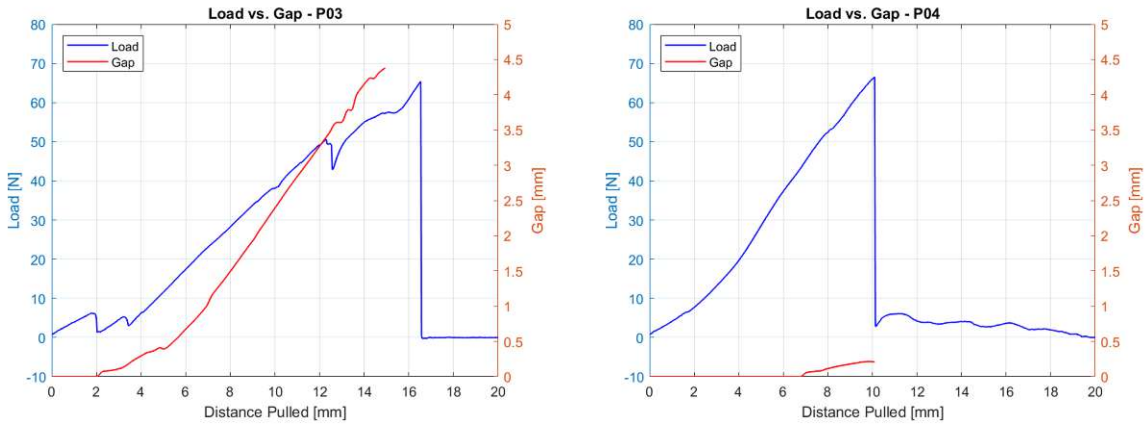

(a) Intra-osseous suture (b) Suture anchor

Figure 29: Load (blue) and gap (red) measurement during testing.

The x-axis represents the distance that is pulled by the tensile testing machine. Due to the constant displacement velocity, it can also be seen as a measure of time. The left y-axis and the blue curve show the load that is measured during testing, while the y-axis on the right and the red curve represent the gap, extracted from the recorded video.

Typically, load development is steeper for the samples prepared by the Weldix® anchor. Comparing the results pairwise, the bigger gap always occurs in the sample prepared by intra-osseous suture. The quantified results are described in the following.

5.2 Load at Characteristic Gap

The mean values of measured force at the time of registration of characteristic gaps between bone and tendon are shown in table 1, along with their standard deviations. n shows the number of occurrences of the respective gap size. If not all 7 samples per group are mentioned, the sample already failed before reaching the desired gap. The P-Value indicates the level of significance after independent t-testing. The result of the pairwise t-test is added for the 0.5 mm gap variable in brackets (Here, at least 5 pairs could be analyzed).

Table 1: Mean load and standard deviation at registration of characteristic gaps of 0.5 mm, 1 mm and 3 mm. * indicates statistical significance.

Variable	Intra-Osseous Suture		Suture Anchor		P-Value
	Load [N]	n	Load [N]	n	
0.5 mm gap	23.0 ± 15.4	7	44.2 ± 5.5	5	0.016* (pw: 0.098)
1 mm gap	28.6 ± 17.1	7	51.3 ± 9.3	3	0.067
3 mm gap	42.4 ± 7.8	6	-	0	-

Already at a gap size of 0.5 mm, differences between both groups are clearly visible. Samples prepared by intra-osseous suture reached this gap at a mean load of (23.0 ± 15.4) N, compared to significantly higher (44.2 ± 5.5) N for anchor samples. Figure 30 shows boxplots of both groups, highlighting the median force at a 0.5 mm gap.

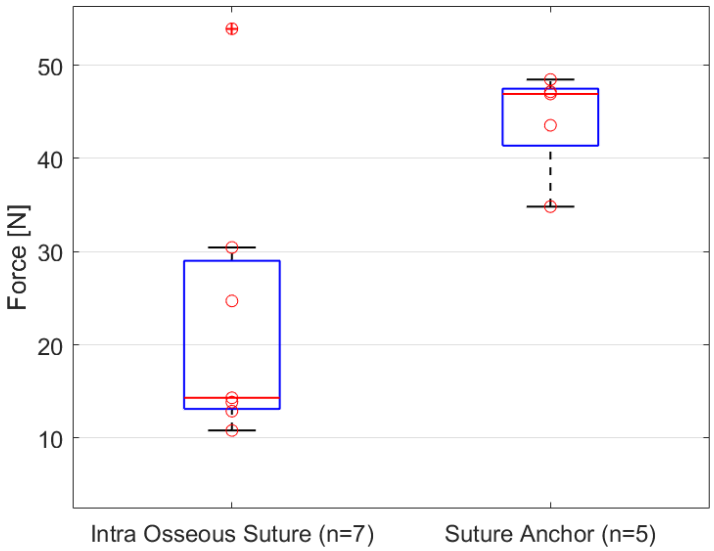

Figure 30: Load at gap-size of 0.5 mm: Intra-osseous suture vs suture anchor. Vertical red line: median value. Box: upper and lower quartiles. Whiskers: minimum or maximum value, if distance between box and value is lower or equal to 1.5 times the interquartile range. Otherwise, data point is visualized as an outlier in this plot.

It is seen, that an outlier in the control group with a measured force of almost 53.9 N (as seen in Appendix A, P13) is responsible for the high standard deviation.

In figure 31 the equivalent boxplot at gap-detection of 1 mm shows a similar picture. Again, the outlier of P13, now measured at 66.3 N, highly influences results.

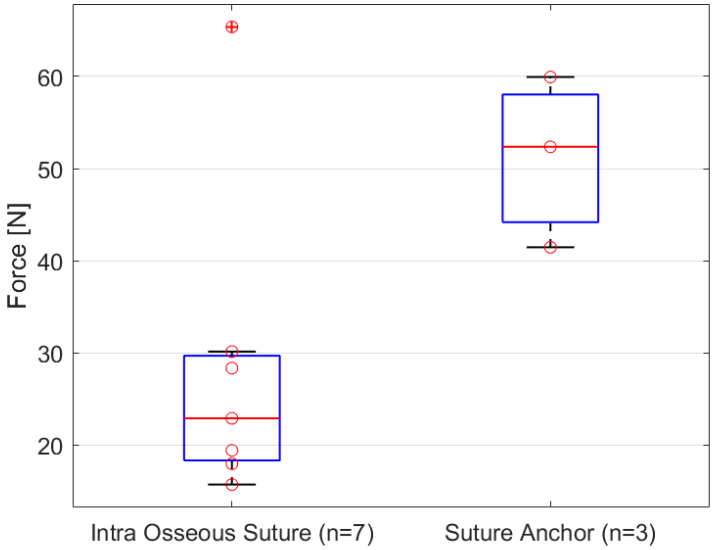

Figure 31: Load at gap-size of 1 mm: Intra-osseous suture vs. suture anchor.

Still, the mean value of the control group is, with (28.6 ± 17.1) N, almost only half as high as the (51.3 ± 9.3) N measured at anchor-repaired tendons. It is even lower than the mean force at 0.5 mm of the suture anchor group. It should be noted, that only three of seven anchor samples were even registered with a gap of 1 mm. The four remaining samples developed relatively high forces before that and the suture failed before reaching a 1 mm gap.

Looking at the 3 mm gap load in table 1, it stands out that no anchor sample reached this gap at all. In comparison, the mean force at intra-osseous sutures is now (42.4 ± 7.8) N. It is interesting, that this value is similar to the load measured in the other group at a gap of 0.5 mm.

5.3 Stress at Characteristic Gap

Equivalent to section 5.2, the mean values of stress are shown in table 2.

Table 2: Mean stress and standard deviation at registration of characteristic gaps of 0.5 mm, 1 mm and 3 mm.

Variable	Intra-Osseous Suture Stress $[N/mm^2]$	n	Suture Anchor Stress $[N/mm^2]$	n	P-Value
0.5 mm gap	1.7 ± 1.0	7	2.7 ± 0.3	5	0.073 (pw: 0.221)
1 mm gap	2.1 ± 1.1	7	3.2 ± 0.5	3	0.14
3 mm gap	3.3 ± 1.0	6	-	0	-

Similarly to force, higher stress is needed to create all gaps within the group of anchor samples. The 0.5 mm gap is reached at a mean stress of (1.7 ± 1.0) N/mm^2 by the control group, while the mean stress is (2.7 ± 0.3) N/mm^2 for the suture anchor group. A gap of 1 mm is measured at a mean stress of (2.1 ± 1.1) N/mm^2 for intra-osseous sutures and at (3.2 ± 0.5) N/mm^2 for anchor samples. The mean stress calculated for the 3 mm gap within the control group is (3.3 ± 1.0) N/mm^2.

Other than for force, the differences in stress are not found to be significant. When looking at figures 32 and 33 and comparing them to figures 30 and 31, it stands out that the interquartile range increases for the intra-osseous suture group. Values that were seen as outliers before are now within the whiskers of the boxplot.

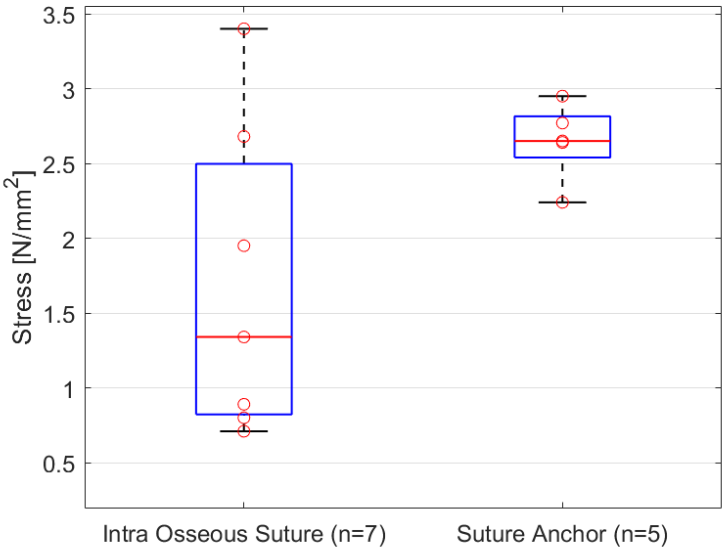

Figure 32: Stress at gap-size of 0.5 mm: Intra-osseous suture vs. suture anchor.

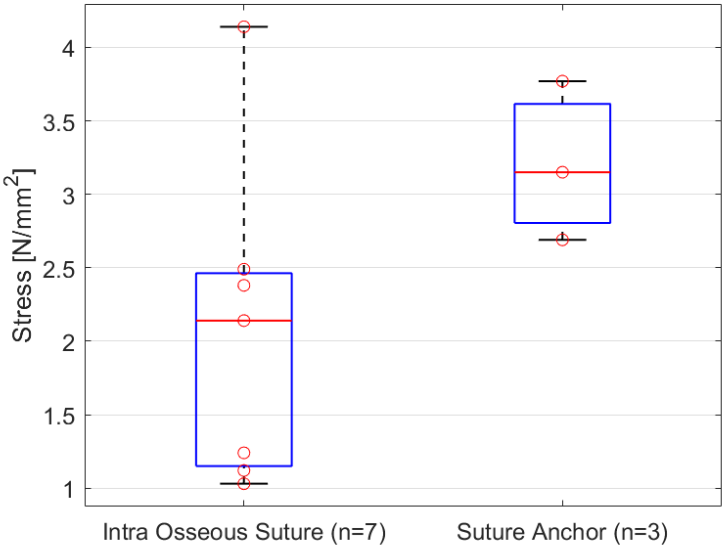

Figure 33: Stress at gap-size of 1 mm: Intra-osseous suture vs. suture anchor.

5.4 Gap at Characteristic Load

To eliminate the problem of having a certain gap only in one group, the reverse approach was taken for this section. Looking at gap registration during the same load that is measured on the tendon resulted in the mean gap values in table 3.

Table 3: Mean gap and standard deviation at load of 30 N and 45 N. * indicates statistical significance.

Variable	Intra-Osseous Suture		Suture Anchor		*P*-Value
	Gap [mm]	n	Gap [mm]	n	
30 N	1.6 ± 0.8	6	0.1 ± 0.1	2	0.058
45 N	2.8 ± 1.3	7	0.5 ± 0.6	6	0.003* (pw: 0.021*)

Similarly to section 5.2, n represents the number of occurrences. Especially at a load of 30 N, there is only a gap visible in two of the seven tested samples, while the control group already shows a clear gap of (1.6 ± 0.8) mm on average. Even the two anchor samples that already show gap development are still at the very beginning of gap formation with values of 0.1 mm and 0.18 mm (P10 & P14). These results are visualized in figure 34 similarly to the previous section.

To include more samples, the same analysis is done at a load of 45 N. By now, already 6 anchor samples developed a gap between bone and tendon. The mean gap in the control group is now (2.8 ± 1.3) mm. This is in line with the findings of section 5.2 in table 1. The suture anchor group is now registered with a mean gap of (0.5 ± 0.6) mm. The high standard deviations in both groups are due to one outlier per group,

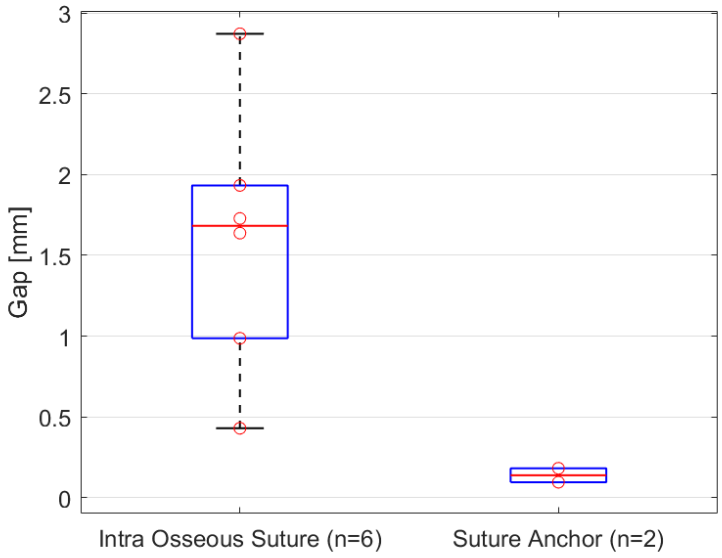

Figure 34: Gap at a load of 30N: Intra-osseous suture vs. suture anchor.

respectively seen in figure 35. Despite those outliers (P13 & P10), the difference in mean value is statistically significant both by looking at independent (P=0.003) and paired (P=0.003) variables.

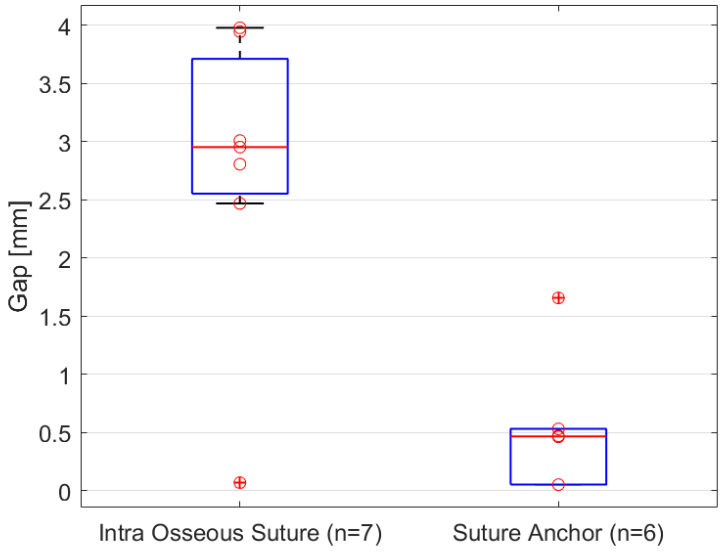

Figure 35: Gap at a load of 45N: Intra-osseous suture vs. suture anchor.

5.5 Maximum Load

In 12 out of 14 cases, the suture failed during testing. For two samples with intra-osseous suture, gap development was so large that the pre-defined displacement of the tensile testing machine was not sufficient to cause suture failure. The mean values of this maximum failure load are listed in table 4.

Table 4: Mean failure load and standard deviation.

Variable	Intra-Osseous Suture Load [N]	n	Suture Anchor Load [N]	n	*P*-Value
Failure	65.1 ± 8.3	5	55.2 ± 8.0	7	0.067 (pw: 0.18)

On average, the failure load at samples with an intra-osseous suture was about 10 N higher than within the anchor group. However, statistically, this difference is not significant difference ($\alpha = 0.05$) with a P-value of 0.067 for independent and 0.18 for a paired t-test.

5.6 Types of Failure

In addition to failure load, the mode of failure was evaluated. During the first two tests, it was observed that both intra-osseous sutures failed close to the knot (figure 36a) and both anchor samples seemed to fail at the contact point of suture and anchor (figure 36b).

(a) (b)

Figure 36: (a) Suture failure in the knot, (b) Suture failure along the suture

Within the remaining tests, suture failure at the contact point of anchor and suture was only observed in one of five tests, resulting in overall 3 samples with a failure mode similar to figure 36b.

5.7 Backflow of Anchor Material

It was observed that in some suture anchor samples, anchor material was pushed back out of the pre-drilled hole during implantation. The most prominent case of this backflow is visualized in figure 37. Because the diameter of the anchor before implantation is bigger than the diameter of the drilled hole, the material must adapt to the given geometry. This is done by liquefication of outer anchor material due to ultrasonic energy application. It was observed that instead of penetrating deeper trabecular tissue, the path of least resistance for the material to flow was back out of the hole to a certain extent. Shape and extent of backflow was irregular, its correlation with implantation temperature and bone porosity is discussed in chapter 6.

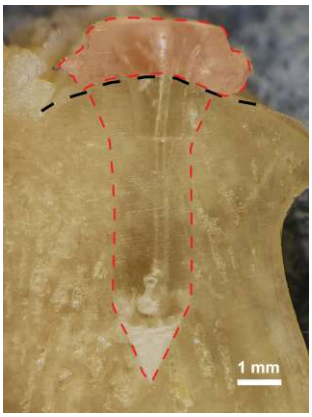

Figure 37: Backflow the anchor material (red) across the bone surface (black).

5.8 Bone Porosity

Bone porosity in the tested anchor samples varied between 7% and 23% with a mean value of (13.5 ± 5.9) %. In figure 38, a linear regression is performed to visualize the correlation between failure load on the x-axis and bone porosity on the y-axis.

The Pearson correlation coefficient is 0.85 with a P-value of 0.0154, indicating that there is a significant positive correlation between both variables. The confidence interval at a level of 0.95 ranges from 0.26 to 0.98.

A look under the microscope at the anchor samples cut into halves shows the anchor's molding behavior. Figures 39a and 39b show anchors in the bones with the highest and lowest porosity. The lowest porosity sample is also the bone shown in section 5.7 with the most prominent case of backflow.

It is observed that the anchor placed in high porosity bone is completely transparent. The low porosity bone shows a white area on the far end of the anchor implant as highlighted by the arrow in figure 39b, possibly indicating poor implantation due to small air inclusions or irregular solidification of the anchor material. This could result

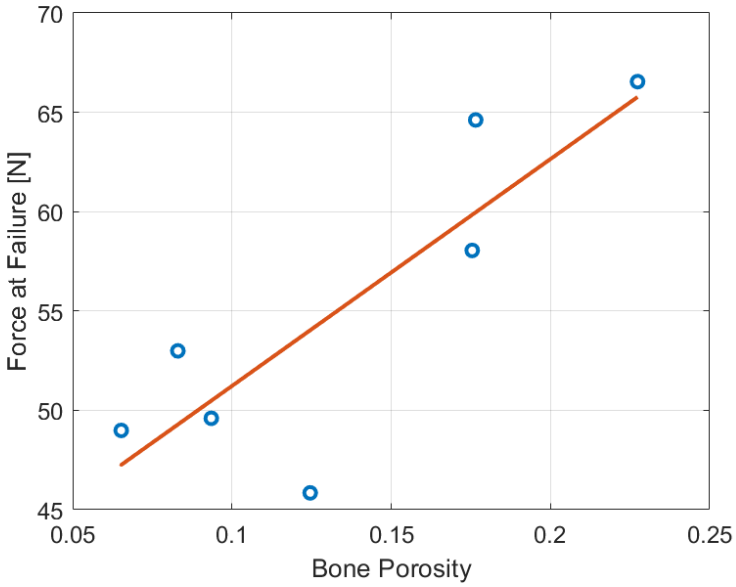

Figure 38: Correlation between Bone Porosity and Maximum Load

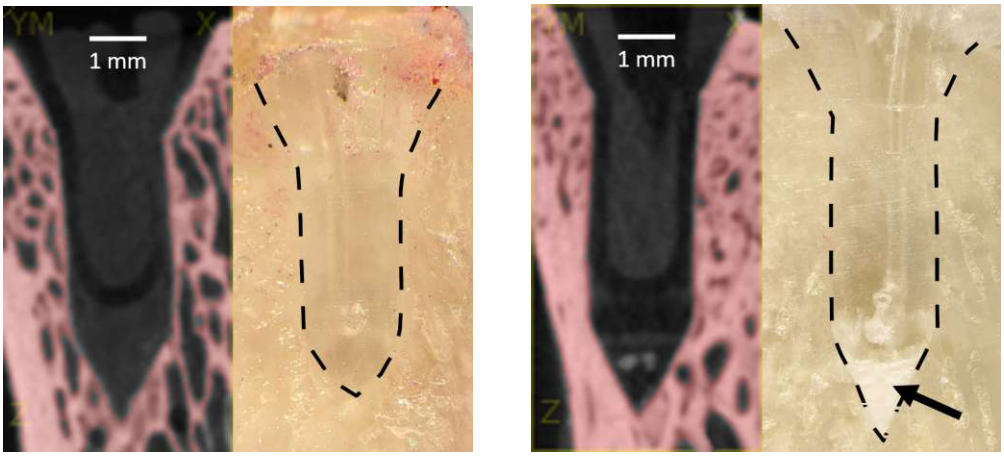

(a) Highest porosity bone (b) Lowest porosity bone

Figure 39: CT image and microscopic view of anchor cross-section. Arrow indicates disturbed anchor material.

in a lack of adhesion between bone and anchor, as the material might not penetrate trabecular structures as expected. The shaft is transparent as other implants. Along the center of the anchor shaft, the outlines of the suture-canal can be observed. In figure 39b, the most distal point of this canal is close to the white area of the anchor. In figure 39b, also the imprint of the ultrasonic implantation sonotrode can be seen in the upper region of the anchor.

Chapter 6

Discussion

6.1 Experimental Tests

Within this work, the biomechanical behaviors of two re-fixation methods for the feline Achilles tendon were tested in-vitro with a custom-built load-displacement testing set-up. Thereby, the load-bearing performance of the VetWelding Weldix® suture anchor was compared to the state-of-the-art intra-osseous suture tunnel as a control group. To simulate physiological loading, the anatomical positions of bone and tendon were taken into account, creating an angle of 125° between the calcaneus and the Achilles tendon. This is in the range of physiological hind leg positioning of cats during the stance phase, as reported by Brown et al. [35].

Two pairs of samples needed to be excluded from the study due to complications during preparation or testing. Due to logistic issues, seven pairs of samples could ultimately be included in the study. Looking at the raw results of gap and load propagation in figures 29a and 29b as well as in most other tests seen in Appendix A, load increase was found to generally be steeper for the suture anchor group when compared to the control group. This effect can be explained by a tighter suture, indicating that less suture material is used for enthesis repair. It was observed, that some intra-osseous sutures tend to show a quick decrease in force at some point during testing. This is especially evident in P05, P09, and P19. By analyzing the videos, it was found that this is due to the suture laterally slipping over epicondyles of the calcaneus. A possible explanation for this behavior is sample preparation, where most of the soft tissue on the proximal calcaneus is removed to enable a clear vision of bone edges. In vivo, soft tissue might reduce the risk of suture slippage, as friction on the calcaneus surface is increased.

In two cases (P05 & P17), the graph for gapping ends before suture failure. Here, the gap grew so large, that the distal tendon end is pulled out of the camera's field of vision. For evaluation of gap size at the point of failure, the field of vision by the

camera might need to be increased.

Results for mean load at characteristic gaps in the group of intra-osseous sutures were found to be similar to earlier results [8]. In the study by Moores et al. [8] on canine Achilles tendons, a 1 mm gap load of (31 ± 4.2) N and a 3 mm gap load of (49.1 ± 2.4) N were measured when using the suturing technique of a modified 3-loop pulley in combination with an intra-osseous suture.

Moores et al. [8] also compared different suturing techniques. With a locking-loop pattern, characteristic gap forces were lower. The Bunnell-Mayer technique used in Moores et al. seems to lay in between those techniques with (28.6 ± 17.1) N (1 mm gap) and (42.4 ± 7.8) N (3 mm gap).

It was observed that samples, prepared with suture anchors, reached a gap of 1 mm only in three of seven cases at forces almost twice as large as within the control group. Anchor samples never reached a gap of 3 mm. In order to still compare both methods, another characteristic gap of 0.5 mm was introduced. Using this, seven results of the intra-osseous suture group could be compared to five values in the suture anchor group. Again, the gap load within the suture anchor group is almost double when compared to the control group (44.2 N vs. 23.0 N), with the difference being statistically significant (P=0.016).

Looking at figures 30 and 31, an outlier in the control group was detected. In this case of P13, only a small gap between bone and tendon was observed, as seen in Appendix A. This outlier is the reason for large standard deviations in characteristic gap forces in the control group, making some results statistically not significant, even though large differences between both tested groups seem to be evident.

During testing, anatomical differences between samples were evident. This led to the idea of comparing not only characteristic gap load but also stress, taking into account geometrical differences of tendons. By comparing figures 32 and 33 to the according graphs above, it can be seen that variation within those groups is actually decreased. Results that were complete outliers when looking at load are now within the whiskers of the boxplots. It is also observed, that differences between both groups seem to decrease. For a more meaningful interpretation, the determination of cross-section has to be revised though, as some tendons are more crimped to the bone than others, leading to possible misinterpretation. For better understanding, the use of characteristic gap forces is still preferred.

To eliminate the problem of having an unequal amount of results for both groups, the reverse approach to Moores et al. [8] was taken by looking at a specific load and comparing gaps found on samples of both groups. It turned out that a force of 30 N is too low to include all samples, as anchor samples have not developed a gap at that point yet. A characteristic load of 45 N yielded better results. Now all seven samples from the control group could be compared to 6 samples with suture anchor. The only

sample excluded here is P16, as there was no gap found at all before failure. Mean values here suggest a statistically significant difference (P=0.003, pairwise P=0.021). Intra-osseous sutures were already measured with a gap of 2.8 mm. Again, P13 is found to be the only outlier, responsible for a high standard deviation of 1.3 mm. When comparing those values with the findings at a characteristic gap load of 3 mm as suggested by Moores et al. [8], the introduction of a characteristic load gap at 45 N seems to be a good alternative. Within the suture anchor group, a mean value of 0.5 mm shows again, that gap development is lower in this group.

An explanation for this is the length of suture used for both methods. While more suture needs to be threaded through the whole diameter of bone and wrapped around epiphyses of the calcaneus, the suture is already fixed at the site of tendon reinsertion when using the suture anchor. Absolute suture displacement clearly depends on absolute suture length, resulting in larger gaps at the same strain when more suture is used.

The seemingly lower failure load within the group of suture anchors is not significant. However, observation of modes of failure seemed to suggest in some cases that the suture is damaged by anchor material during implantation or testing and the failure load could be even higher. The intention of the BoneWelding® technology is to penetrate the trabecular structure with the anchor polymer material during implantation. In some cases, backflow of anchor material was observed. This means that anchor material was protruding out of the pre-drilled hole after implantation. During implantation, anchor material liquefies and adapts to the geometry of the hole. After the hole was filled, it seemed like the path of least resistance for material to flow was back out of the hole instead of penetrating deeper trabecular structures. This could lead to sharp edges of anchor material that could induce suture damage upon load. Resistance against penetration of trabecular structures by polymer could also influence the handling of the implantation sonotrode during the preparation process. If the sonotrode is pushed too far into the anchor, the suture might get damaged. An important factor for the resistance against penetration of trabecular structures by polymer is the temperature during implantation. The anchor material has a distinct temperature window of liquefaction. Bone samples used for this study were generally prepared at room temperature, some samples might have been prepared below room temperature. The difference of more than 10°C compared to the in vivo application could very well have influenced anchor liquefication, leading to less penetration and more backflow. Another factor that could influence resistance against penetration is bone porosity. High porosity allows more material to be embedded in the trabecular structure, possibly prohibiting backflow, irregular implantation as seen in figure 39b, or suture damage by mishandling of the sonotrode. Ultimately, a Pearson correlation coefficient of 0.85 between bone porosity and failure load already shows statistical significance, however,

more samples could solidify this early finding.

In general, the failure load of both tested methods for tendon re-fixation is below the load that can physiologically occur within healthy cats. The use of splints or fixation screws is definitely required to minimize load on the Achilles tendon after surgery to less than 45 N, with that being the minimal failure load found in this study.

Other than that, when it comes to gap propagation, the findings of this work suggest that the biomechanical performance of the VetWelding suture anchor is preferred over the performance of intra-osseous suture tunnels.

6.2 Limitations & Future Work

For now, a set of seven pairs of feline Achilles tendons was tested. In order to create more stable results, and to put outliers into context, an increased sample size would be necessary. Especially for pairwise comparison, too few samples were tested, as some characteristic values are not even reached by some samples due to large differences in gap propagation.

For sample preparation by the Weldix® suture anchor, the bone temperature during implantation needs to be considered. For this study, samples were prepared at room temperature, some samples might have been below room temperature during anchor implantation. Future sample preparation could be performed in a water bath at constant body temperature, ensuring implantation conditions as in vivo. This is expected to minimize backflow and the lack of trabecular penetration and could possibly increase failure load.

The gap between bone and tendon was analyzed only in one plane. Even though this is sufficient once the complete separation of bone and tendon is found, an additional camera could increase precision by looking at another plane, especially in the region of gaps up to 0.5 mm. Because gaps with the suture anchor seem to be very small, this might be a good addition for future studies.

In vivo, the repaired tendon is not exposed to linear, but to cyclic loading. Future studies might take that into account and investigate gap formation upon repetitive load, well under the failure load found in this study. For that, it is important to know the forces that act on the suture when the cat's leg is splinted. Simulation studies or clinical tests could give an answer to this question in the future.

6.3 Conclusion

The goal of this work was to establish and conduct an experiment to evaluate the biomechanical performance of the VetWelding Weldix® suture anchor compared to an intra-osseous suture applied to feline Achilles tendon ruptures. Comparing the results of the control group to similar studies suggests that the experimental setup and data analysis protocol work. The comparative results of both tested groups show that the biomechanical properties of the VetWelding Weldix® suture anchor are superior to the current state-of-the-art intra-osseous suture. Especially, gapping between bone and tendon can be minimized by using the new method, leading to better prospects of healing. Failure loads suggest that splints or fixation screws are essential to reduce the risk of suture failure. Future research on the developed experimental setup can be done to increase the statistical power of the findings. Also, different approaches such as cyclic loading of the repaired tendon could be investigated, to create a better understanding of feline Achilles tendon injuries.

Appendix A

Results

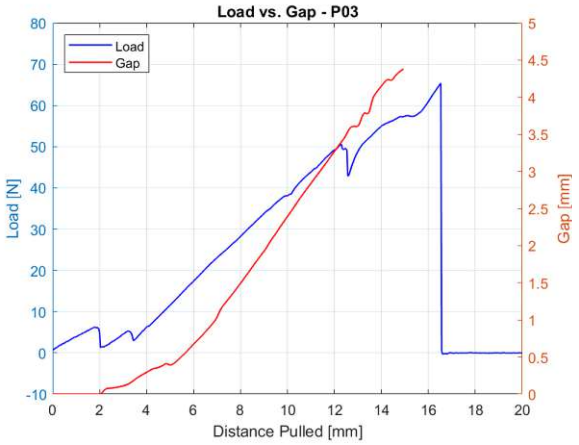

(a) Intra Osseous Suture - P03

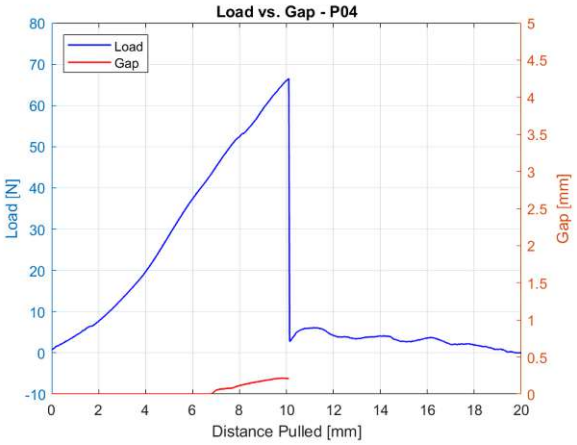

(b) Suture Anchor - P04

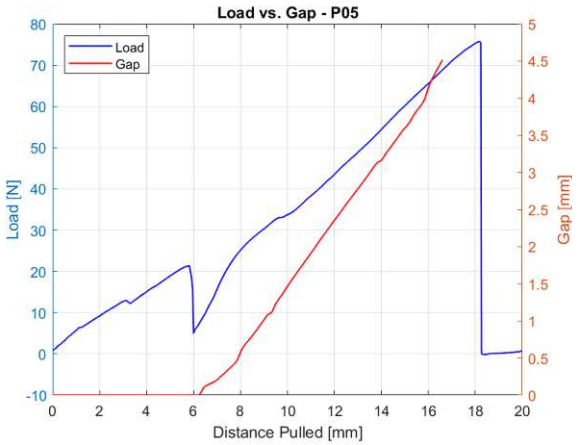

(a) Intra Osseous Suture - P05

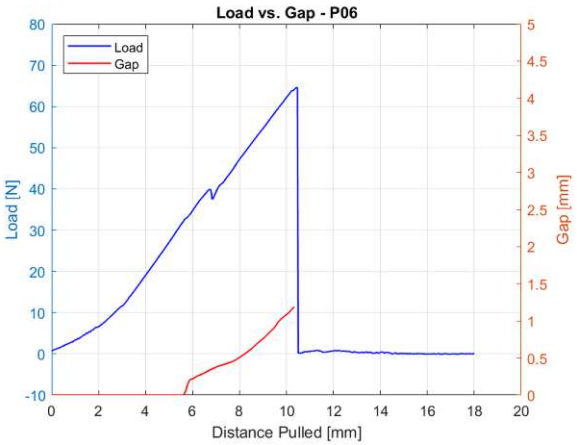

(b) Suture Anchor - P06

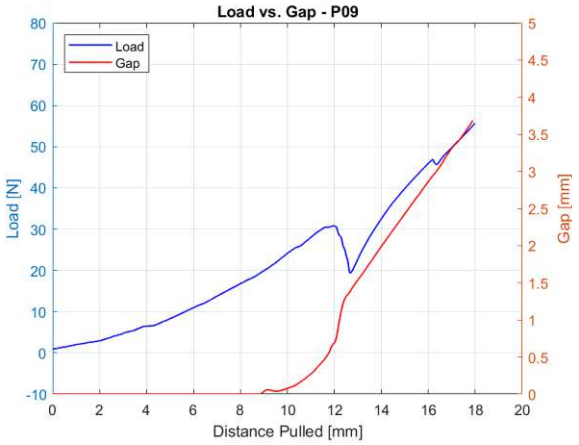

(a) Intra Osseous Suture - P09

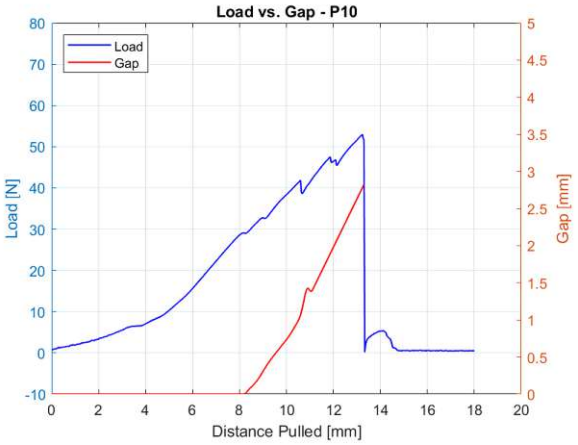

(b) Suture Anchor - P10

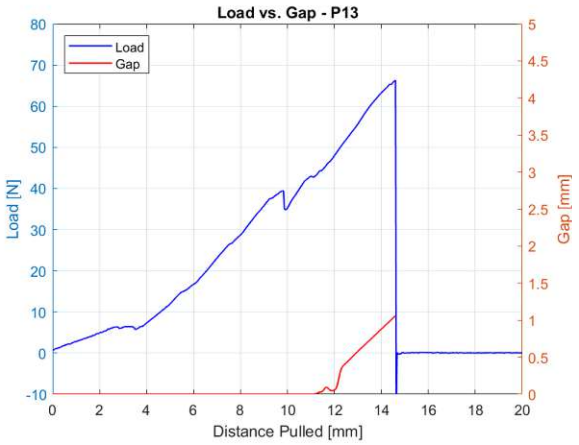

(a) Intra Osseous Suture - P13

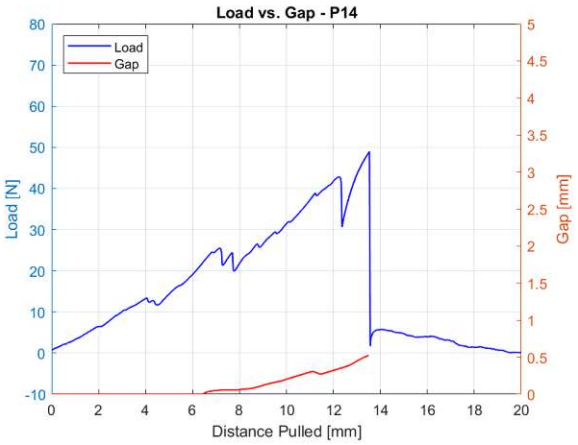

(b) Suture Anchor - P14

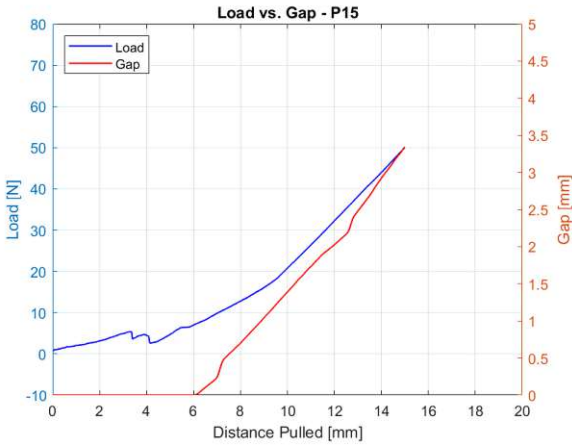

(a) Intra Osseous Suture - P15

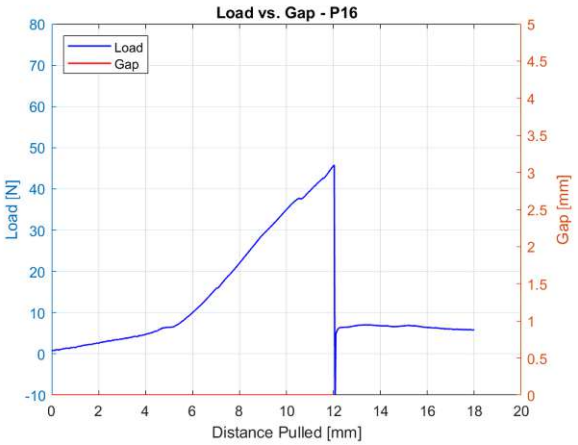

(b) Suture Anchor - P16

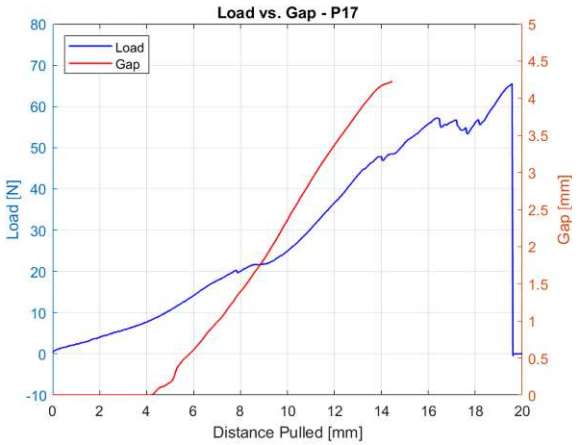

(a) Intra Osseous Suture - P17

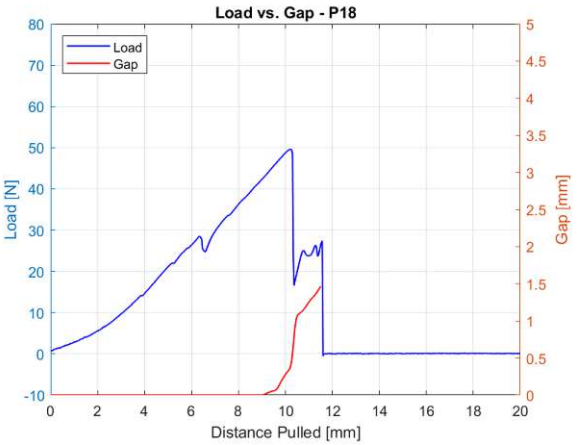

(b) Suture Anchor - P18

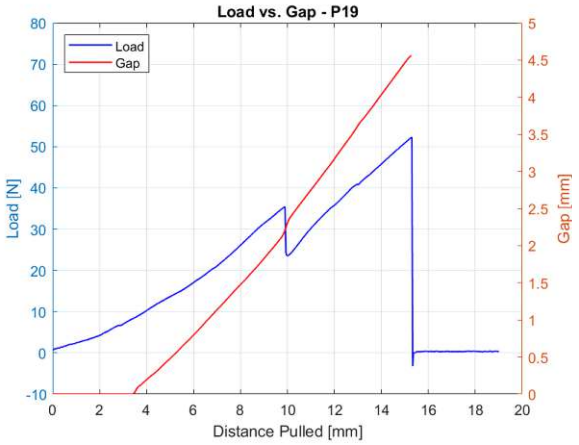

(a) Intra Osseous Suture - P19

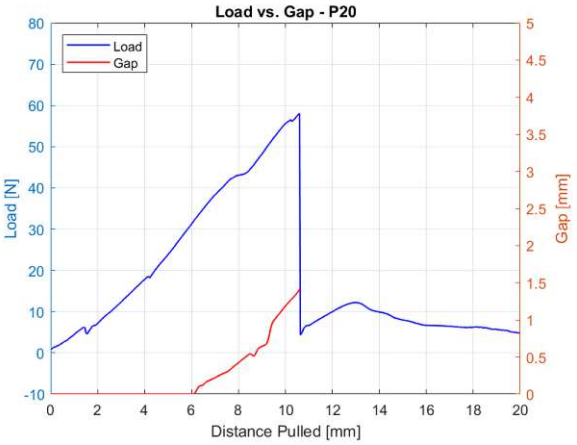

(b) Suture Anchor - P20

Bibliography

[1] M. Cervi, N. Brebner, and J. Liptak. Short- and long-term outcomes of primary Achilles tendon repair in cats: 21 Cases. *Veterinary and Comparative Orthopaedics and Traumatology*, 23(05):348–353, 2010. Publisher: Schattauer GmbH.

[2] A. Mughannam and J. Reinke. Avulsion of the gastrocnemius tendon in three cats. *American Animal Hospital Association (USA)*, 1994.

[3] P. M. Montavon, K. Voss, and S. J. Langley-Hobbs. *Feline orthopedic surgery and musculoskeletal disease*. Saunders, Edinburgh, 1. ed.. edition, 2009. ISBN 978-0-7020-2986-8.

[4] G. Arthurs, G. Brown, and R. Pettitt. *BSAVA manual of canine and feline musculoskeletal disorders: a practical guide to lameness and joint disease*. BSAVA manuals series. British Small Animal Veterinary Association, Quedgeley, Gloucester, second edition. edition, 2018. ISBN 978-1-905319-69-5.

[5] L. E. Visscher, C. Jeffery, T. Gilmour, L. Anderson, and G. Couzens. The history of suture anchors in orthopaedic surgery. *Clinical Biomechanics*, 61:70–78, Jan. 2019.

[6] R. M. Barros, M. A. Matos, A. A. Ferreira Neto, E. Benegas, R. Guarniero, C. A. M. Pereira, and R. Bolliger Neto. Biomechanical evaluation on tendon reinsertion by comparing trans-osseous suture and suture anchor at different stages of healing: experimental study on rabbits. *Journal of Shoulder and Elbow Surgery*, 19(6):878–883, Sept. 2010.

[7] BoneWelding® technology sets new standards in animal orthopedics, 2022. URL `https://www.vetwelding.com/technology/`.

[8] A. P. Moores, E. J. Comerford, J. F. Tarlton, and M. R. Owen. Biomechanical and Clinical Evaluation of a Modified 3-Loop Pulley Suture Pattern for Reattachment of Canine Tendons to Bone. *Veterinary Surgery*, 33(4):391–397, July 2004.

[9] R. H. Gelberman, M. I. Boyer, M. D. Brodt, S. C. Winters, and M. J. Silva. The effect of gap formation at the repair site on the strength and excursion of

intrasynovial flexor tendons. An experimental study on the early stages of tendon-healing in dogs. *The Journal of Bone and Joint Surgery. American Volume*, 81 (7):975–982, July 1999.

[10] P. Thurner. Tissue Biomechanics [lecture notes]. *TU Wien*, 2020.

[11] S. C. Cowin, editor. *Bone Mechanics Handbook*. CRC Press, Boca Raton, 2 edition, 2001. ISBN 978-0-429-12544-7.

[12] S. Weiner and D. Wagner. The Material Bone: Structure-Mechanical Function Relations. *Annual Review of Materials Research*, 28:271–298, Nov. 2003.

[13] M. Sadat-Shojai, M.-T. Khorasani, E. Dinpanah-Khoshdargi, and A. Jamshidi. Synthesis methods for nanosized hydroxyapatite with diverse structures. *Acta Biomaterialia*, 9(8):7591–7621, Aug. 2013.

[14] M.-C. Monier-Faugere, M. Chris Langub, and H. H. Malluche. Chapter 8 - Bone Biopsies: A Modern Approach. In L. V. Avioli and S. M. Krane, editors, *Metabolic Bone Disease and Clinically Related Disorders (Third Edition)*, pages 237–280e. Academic Press, San Diego, Jan. 1998. ISBN 978-0-12-068700-8.

[15] P. Fratzl, H. Gupta, L. Paschalis, and P. Roschger. Structure and mechanical quality of the collagen-mineral nano-composite in bone. *J. Mater. Chem.*, 14, July 2004.

[16] V. C. Mow. *Basic orthopaedic biomechanics & mechano-biology*. Lippincott Williams & Wilkins, Philadelphia, Pa. [u.a.], 3. ed.. edition, 2005. ISBN 978-0-7817-3933-7.

[17] J. D. Black and B. J. Tadros. Bone structure: from cortical to calcium. *Orthopaedics and Trauma*, 34(3):113–119, June 2020.

[18] M. Nordin and V. H. Frankel. *Basic Biomechanics of the Musculoskeletal System*. Lippincott Williams \& Wilkins, 2001.

[19] C. J. Collins, O. G. Andriotis, V. Nedelkovski, M. Frank, O. L. Katsamenis, and P. J. Thurner. Bone Micro- and Nanomechanics. In R. Narayan, editor, *Encyclopedia of Biomedical Engineering*, pages 22–44. Elsevier, Oxford, Jan. 2019. ISBN 978-0-12-805144-3.

[20] P. J. Thurner. Atomic force microscopy and indentation force measurement of bone. *WIREs Nanomedicine and Nanobiotechnology*, 1(6):624–649, 2009.

[21] E. F. Morgan, G. U. Unnikrisnan, and A. I. Hussein. Bone Mechanical Properties in Healthy and Diseased States. *Annual review of biomedical engineering*, 20: 119–143, June 2018.

[22] M. Frank, A. G. Reisinger, D. H. Pahr, and P. J. Thurner. Effects of Osteoporosis on Bone Morphometry and Material Properties of Individual Human Trabeculae in the Femoral Head. *JBMR Plus*, 5(6):e10503, 2021.

[23] H. R. C. Screen, D. L. Bader, D. A. Lee, and J. C. Shelton. Local Strain Measurement within Tendon. *Strain*, 40(4):157–163, 2004.

[24] K. Barfod. Achilles tendon rupture; Assessment of nonoperative treatment. *Danish medical journal*, 61, Apr. 2014.

[25] C. N. Maganaris and J. P. Paul. In vivo human tendon mechanical properties. *The Journal of Physiology*, 521 Pt 1:307–313, Nov. 1999.

[26] E. Thomas. Tendon Biomechanics, 2022. URL `https://www.physio-pedia.com/Tendon_Biomechanics`.

[27] M. Benjamin and J. R. Ralphs. Entheses–the bony attachments of tendons and ligaments. *Italian Journal of Anatomy and Embryology = Archivio Italiano Di Anatomia Ed Embriologia*, 106(2 Suppl 1):151–157, 2001.

[28] M. BENJAMIN and J. R. RALPHS. Fibrocartilage in tendons and ligaments — an adaptation to compressive load. *Journal of Anatomy*, 193(Pt 4):481–494, Nov. 1998.

[29] J. Apostolakos, T. J. Durant, C. R. Dwyer, R. P. Russell, J. H. Weinreb, F. Alaee, K. Beitzel, M. B. McCarthy, M. P. Cote, and A. D. Mazzocca. The enthesis: a review of the tendon-to-bone insertion. *Muscles, Ligaments and Tendons Journal*, 4(3):333–342, Nov. 2014.

[30] S. C. Cowin. *Tissue mechanics*. Springer, New York, NY, 2007. ISBN 978-0-387-36825-2.

[31] A. S. Tadros, B. K. Huang, and M. N. Pathria. Muscle-Tendon-Enthesis Unit. *Seminars in Musculoskeletal Radiology*, 22(3):263–274, July 2018. Publisher: Thieme Medical Publishers.

[32] M. Benjamin, T. Kumai, S. Milz, B. M. Boszczyk, A. A. Boszczyk, and J. R. Ralphs. The skeletal attachment of tendons–tendon "entheses". *Comparative Biochemistry and Physiology. Part A, Molecular & Integrative Physiology*, 133(4): 931–945, Dec. 2002.

[33] A. Selvanetti, M. Cipolla, and G. Puddu. Overuse tendon injuries: Basic science and classification. *Operative Techniques in Sports Medicine*, 5(3):110–117, July 1997.

[34] F. Ruppert and A. Badri-Spröwitz. Series Elastic Behavior of Biarticular Muscle-Tendon Structure in a Robotic Leg. *Frontiers in Neurorobotics*, 13:64, 2019.

[35] N. P. Brown, G. E. Bertocci, K. A. Cheffer, and D. R. Howland. A three dimensional multiplane kinematic model for bilateral hind limb gait analysis in cats. *PLOS ONE*, 13(8):e0197837, Aug. 2018. Publisher: Public Library of Science.

[36] R. J. Gregor, D. W. Smith, and B. I. Prilutsky. Mechanics of slope walking in the cat: quantification of muscle load, length change, and ankle extensor EMG patterns. *Journal of Neurophysiology*, 95(3):1397–1409, Mar. 2006.

[37] B. de la Torre Valdovinos, J. M. Duenas Jimenez, I. J. Estrada, J. Banuelos Pineda, N. E. Franco Rodriguez, J. R. Lopez Ruiz, L. P. Osuna Carrasco, A. Candanedo Arellano, and S. H. Duenas Jimenez. Tamoxifen Promotes Axonal Preservation and Gait Locomotion Recovery after Spinal Cord Injury in Cats. *Journal of Veterinary Medicine*, 2016:e9561968, Feb. 2016. Publisher: Hindawi.

[38] M. A. Boin, M. A. Dorweiler, C. J. McMellen, G. C. Gould, and R. T. Laughlin. Suture-Only Repair Versus Suture Anchor-Augmented Repair for Achilles Tendon Ruptures With a Short Distal Stump: A Biomechanical Comparison. *Orthopaedic Journal of Sports Medicine*, 5(1):2325967116678722, Jan. 2017.

[39] H. W. Scott, J. Marti, and P. Witte. *Feline orthopedics*. CRC Press, Boca Raton, second edition. edition, 2022. ISBN 978-1-4987-6497-1.

[40] S. Klingler and F. Forterre. Achillessehnenrupturen bei Hunden und Katzen – allgemeine Therapiegrundsätze. *kleintier konkret*, 19(06):19–25, Dec. 2016.

[41] S. Bunnell. Repair of tendons in the fingers and description of two new instruments. *Surg Gynecol Obstet*, 26:103–110, 1918.

[42] C. Zhao, P. C. Amadio, M. E. Zobitz, and K. N. An. Gliding characteristics of tendon repair in canine flexor digitorum profundus tendons. *Journal of Orthopaedic Research: Official Publication of the Orthopaedic Research Society*, 19(4):580–586, July 2001.

[43] S. Rawson, S. Cartmell, and J. Wong. Suture techniques for tendon repair; a comparative review. *Muscles, ligaments and tendons journal*, 3:220–228, July 2013.

[44] Y. Dogramaci, A. Kalaci, T. T. Sevinç, E. Esen, M. Komurcu, and A. N. Yanat. Does strand configuration and number of purchase points affect the biomechanical behavior of a tendon repair? A biomechanical evaluation using different kessler methods of flexor tendon repair. *Hand (New York, N.Y.)*, 3(3):266–270, Sept. 2008.

[45] S. C. Zatiti, N. Mazzer, and C. H. Barbieri. Mechanical strengths of tendon sutures. An in vitro comparative study of six techniques. *Journal of Hand Surgery (Edinburgh, Scotland)*, 23(2):228–233, Apr. 1998.

[46] M. C. Jordan, S. Hoelscher-Doht, K. Fehske, F. Gilbert, H. Jansen, and R. H. Meffert. Bunnell or cross-lock Bunnell suture for tendon repair? Defining the biomechanical role of suture pretension. *Journal of Orthopaedic Surgery and Research*, 10:192, Dec. 2015.

[47] Weldix® 2.3mm Anchor - VetWelding AG, 2022. URL `https://www.vetwelding.com/products-and-solutions/weldix-anchor/`.

[48] M. Ettinger, A. Dratzidis, C. Hurschler, S. Brand, T. Calliess, C. Krettek, M. Jagodzinski, and M. Petri. Biomechanical Properties of Suture Anchor Repair Compared With Transosseous Sutures in Patellar Tendon Ruptures A Cadaveric Study. *The American journal of sports medicine*, 41, Aug. 2013.

[49] F. A. Barber, M. A. Herbert, R. C. Beavis, and F. Barrera Oro. Suture Anchor Materials, Eyelets, and Designs: Update 2008. *Arthroscopy: The Journal of Arthroscopic & Related Surgery*, 24(8):859–867, Aug. 2008.

[50] R. A. Pedowitz, D. W. Weichel, and F. A. Barber. Implant Choices: The Biomechanics of Anchors and Sutures, 2015.

[51] S. . Nephew. New Q-FIX™ All-Suture Anchor from Smith & Nephew provides surgeons the pull-out strength of a hard implant in half the space, 2015. URL `https://www.prnewswire.com/news-releases/new-q-fix-all-suture-anchor-from-smith--nephew-provides-surgeons-the-pull-out-strength-of-a-hard-implant-in-half-the-space-300055444.html`.

[52] E. M. Goble, W. K. Somers, R. Clark, and R. E. Olsen. The Development of Suture Anchors for Use in Soft Tissue Fixation to Bone. *The American Journal of Sports Medicine*, 22(2):236–239, Mar. 1994. Publisher: SAGE Publications Inc STM.

[53] Y. Ono, J. M. Woodmass, A. A. Nelson, R. S. Boorman, G. M. Thornton, and I. K. Y. Lo. Knotless anchors with sutures external to the anchor body may be

at risk for suture cutting through osteopenic bone. *Bone & Joint Research*, 5(6): 269–275, June 2016. Publisher: The British Editorial Society of Bone & Joint Surgery.

[54] D. Ntalos, K. Sellenschloh, G. Huber, D. Briem, K. Püschel, M. M. Morlock, K.-H. Frosch, F. Fensky, and T. O. Klatte. Conventional rotator cuff versus all-suture anchors—A biomechanical study focusing on the insertion angle in an unlimited cyclic model. *PLOS ONE*, 14(11):e0225648, Nov. 2019. Publisher: Public Library of Science.

[55] F. A. Barber and M. A. Herbert. All-Suture Anchors: Biomechanical Analysis of Pullout Strength, Displacement, and Failure Mode. *Arthroscopy: The Journal of Arthroscopic & Related Surgery*, 33(6):1113–1121, June 2017.

[56] T. Dwyer, T. L. Willett, A. P. Dold, M. Petrera, D. Wasserstein, D. B. Whelan, and J. S. Theodoropoulos. Maximum load to failure and tensile displacement of an all-suture glenoid anchor compared with a screw-in glenoid anchor. *Knee surgery, sports traumatology, arthroscopy: official journal of the ESSKA*, 24(2):357–364, Feb. 2016.

[57] M. F. Güleçyüz, C. Schröder, M. F. Pietschmann, S. Göbel, M. Lehmann, J. Mayer, A. Ficklscherer, V. Jansson, and P. E. Müller. Novel ultrasound assisted suture anchor system using the BoneWelding® technology yields a comparable primary stability in osteopenic and healthy human humeri as a benchmark anchor. *Acta Orthopaedica Et Traumatologica Turcica*, 52(2):127–133, Mar. 2018.

[58] T. Kastenberger, P. Kaiser, G. Schmidle, K. Stock, S. Benedikt, and R. Arora. Clinical results of the BoneWelding®Fiji® anchor for the treatment of Stener lesions of the thumb. *Archives of Orthopaedic and Trauma Surgery*, 141(9):1499–1507, Sept. 2021.

[59] C.-H. Cho, K.-C. Bae, and D.-H. Kim. Biomaterials Used for Suture Anchors in Orthopedic Surgery. *Clinics in Orthopedic Surgery*, 13(3):287–292, Sept. 2021.

[60] S. J. Nho, M. T. Provencher, S. T. Seroyer, and A. A. Romeo. Bioabsorbable anchors in glenohumeral shoulder surgery. *Arthroscopy: The Journal of Arthroscopic & Related Surgery: Official Publication of the Arthroscopy Association of North America and the International Arthroscopy Association*, 25(7):788–793, July 2009.

[61] J. W. Durham, S. A. Montelongo, J. L. Ong, T. Guda, M. J. Allen, and A. Rabiei. Hydroxyapatite coating on PEEK implants: biomechanical and histological study in a rabbit model. *Materials science & engineering. C, Materials for biological applications*, 68:723–731, Nov. 2016.

[62] F. A. Barber. Biodegradable Materials: Anchors and Interference Screws. *Sports Medicine and Arthroscopy Review*, 23(3):112–117, Sept. 2015.

[63] D. Shi, D. Wang, C. Wang, and A. Liu. A novel, inexpensive and easy to use tendon clamp for in vitro biomechanical testing. *Medical Engineering & Physics*, 34(4):516–520, May 2012.

[64] M. Jiang, Z. T. Lawson, V. Erel, S. Pervere, T. Nan, A. B. Robbins, A. D. Feed, and M. R. Moreno. Clamping soft biologic tissues for uniaxial tensile testing: A brief survey of current methods and development of a novel clamping mechanism. *Journal of the Mechanical Behavior of Biomedical Materials*, 103, Mar. 2020.

[65] A. P. Moores, M. R. Owen, and J. F. Tarlton. The three-loop pulley suture versus two locking-loop sutures for the repair of canine achilles tendons. *Veterinary surgery: VS*, 33(2):131–137, Apr. 2004.

[66] M. Petri, M. Ettinger, A. Dratzidis, E. Liodakis, S. Brand, U. V. Albrecht, C. Hurschler, C. Krettek, and M. Jagodzinski. Comparison of three suture techniques and three suture materials on gap formation and failure load in ruptured tendons: a human cadaveric study. *Archives of Orthopaedic and Trauma Surgery*, 132(5):649–654, May 2012.

[67] A. B. Putterman, D. J. Duffy, M. E. Kersh, H. Rahman, and G. E. Moore. Effect of a continuous epitendinous suture as adjunct to three-loop pulley and locking-loop patterns for flexor tendon repair in a canine model. *Veterinary surgery: VS*, 48(7):1229–1236, Oct. 2019.

[68] C. J. Cocca, D. J. Duffy, M. E. Kersh, W. Kim, A. Groenewold, and G. E. Moore. Biomechanical comparison of three epitendinous suture patterns as adjuncts to a core locking loop suture for repair of canine flexor tendon injuries. *Veterinary surgery: VS*, 48(7):1245–1252, Oct. 2019.

[69] A. E. Dunlap, S. E. Kim, and W. T. McNicholas. Biomechanical evaluation of a non-locking pre-manufactured loop suture technique compared to a three-loop pulley suture in a canine calcaneus tendon avulsion model. *Veterinary and Comparative Orthopaedics and Traumatology: V.C.O.T*, 29(2):131–135, 2016.